Automation in Construction 141 (2022) 104406

Contents lists available at ScienceDirect

Automation in Construction

journal homepage: www.elsevier.com/locate/autcon

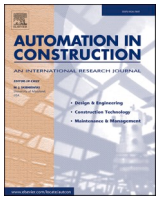

Underpass clearance checking in highway widening projects using digital twins

Feng Jiang [a], Ling Ma [a,*], Tim Broyd [a], Ke Chen [b], Hanbin Luo [b]

[a] The Bartlett School of Sustainable Construction, University College London, London WC1E 6BT, UK
[b] School of Civil and Hydraulic Engineering, Huazhong University of Science and Technology, Wuhan 430074, China

ARTICLE INFO

Keywords:
Digital twin
Road widening
Clearance check
Underpass
Building information modelling
Alignment fitting
Digital terrain model (DTM)

ABSTRACT

Main road widening can reduce the clearance of the low-level underpass road, restricting the passage of vehicles and leading to collisions with structures. Therefore, checking the clearance of the underpass road effectively should be considered at the design stage. This paper describes a digital twin approach for checking the clearance of underpass roads in highway widening projects using online map data. The underpass road digital twin and BIM model of the newly widened road based on the existing main road digital twin are created to assist the clearance check and redesign. The proposed method presented a cost-effective clearance check for underpass roads in road widening design without field surveys and was successfully implemented in an underpass road in the UK. In future research, more digital twin methods for overpasses, bridges, tunnels, and traffic safety facilities should be employed comprehensively to assist more road widening applications.

1. Introduction

Many existing roads cannot meet the up-to-date traffic demands in modern society since they were designed according to the past traffic conditions [20]. Road widening is one of the most effective methods to improve the level of service (LOS) of roads [42]. However, road widening projects can significantly influence the surroundings along the target road, such as building demolition, reconstruction of the crossing roads, pipeline relocation, etc. [1,4,10]. In many cases, several low-level roads cross the main road upwards or downwards [11], and the main road goes over some low-level underpass roads by bridges or culverts. Therefore, sufficient clearance should be reserved for the underpass roads to ensure that vehicles and people can safely go via the underpasses [48]. However, the clearance of an underpass road can significantly constrain road widening projects. The primary reason is the comprehensive effect caused by road widening, the cross fall of the existing main road, and the vertical alignment of the underpass road, as shown in ①, ②, ③ in Fig. 1. The main road is widened, and the cross fall of the main road can lower the edge of the main road. In addition, the low-level underpass road can fall on one side and rise on the other side, controlled by its vertical alignment. Sometimes, the widened part of the main road is constructed over the rising side of the low-level underpass road, reducing the clearance of the low-level underpass road. Furthermore, the settlement of piers and deflection of girders can reduce the clearance of the low-level underpass road, as shown in ④, ⑤ in Fig. 1 [3,9]. Thus, it is necessary to check the clearances of low-level underpass roads after widening the main road.

Road widening should be conducted based on the status of the existing road. The data relating to low-level underpass roads is also essential to check the clearance. However, the design and construction documents of the existing main road and the low-level underpass road cannot always be available, hindering the road widening process [33]. Thus, it is necessary to collect data on the existing main road and the low-level underpass road and reconstruct the digital models of the roads to assist the road widening process and the clearance check. In the preliminary design stage of road widening, conducting a field survey and detailed design is time-consuming and costly [50]. Data such as digital surface model (DSM), digital elevation model (DEM), and aerial photographs can be downloaded from online databases to assist designers in proposing preliminary design schemes [28].

Digital Twin (DT) paradigm is an ideal tool to assist road widening projects. DT is a set of virtual information constructs that fully describes a potential or actual physical manufactured product from the micro atomic level to the macro geometrical level. At its optimum, any information obtained from inspecting a physically manufactured product can be obtained from its DT [21]. At the design stage, the DT can provide

* Corresponding author.
E-mail address: l.ma@ucl.ac.uk (L. Ma).

https://doi.org/10.1016/j.autcon.2022.104406
Received 24 March 2022; Received in revised form 26 May 2022; Accepted 2 June 2022
Available online 9 June 2022

digital replicas for the existing related projects, surroundings, and environment to assist in decision making and designing by collecting data from the physical world and parsing data into understandable expressions [27]. Based on the DT, the widening of the main road and the clearance check of the low-level underpass can be conducted. In addition to field surveys, using secondary data like online map data to build the DT of existing roads is a cost-effective method at the preliminary design stage.

This research proposes a DT-based method to realise clearance checks and redesign the low-level underpass road at the preliminary design stage of the main road widening project. This research focuses not only on the existing main road but also on checking and updating the low-level underpass roads along the main road, which are usually ignored by previous studies. As a result, several research challenges will be solved:

1) How to build the DT of the existing main road and the low-level underpass road using online map data?
2) How to conduct road widening based on the DT of the existing main road?
3) How to realise preliminary clearance check and redesign of the low-level underpass road based on the road widening model and the DT.

The remaining sections of this paper are organised as follows: Section 2 is a systematic literature review of digital twin applications in road engineering and the research related to highway clearance. Section 3 is a detailed introduction of the proposed method. Section 4 is a case study based on the underpass at the intersection of the M11 motorway and Sawbridgeworth Road in Essex County, UK, using the proposed method. Finally, sections 5 and 6 present discussions and conclusions.

2. Literature review

2.1. Digital twin for road engineering

A road is a long-shape infrastructure, and its digital twin method is quite different from structural entities [34]. Nevertheless, existing studies have employed DT in road engineering design, operation and maintenance phases, such as urban planning and road maintenance.

First, some studies only focus on building the DT for existing roads. Justo, et al. [31] proposed a semi-automatic method to extract and establish the road element model following the IFC 4.1 standard from point clouds, such as road alignment, traffic signs, guardrails, and some semantics by property sets. Barazzetti, et al. [2] developed a two-step procedure to detect and classify roads automatically from LiDAR data. Jiang, et al. [28] proposed a systematic and cost-effective highway DT method based on online map data by digital image processing, horizontal alignment fitting, vertical alignment fitting, and cross-section processing. The highway DT considers the primary elements of the highway, such as alignments, central reserves, hard strips, lanes, hard shoulders, verges, and side slopes. Meža, et al. [38] presented a systematic method to establish a fully functioning DT of a road constructed using secondary raw materials. An integrated data environment synthesising a digital model and monitored data is established. Intignano, et al. [25] proposed a systematic workflow based on the Heritage-BIM (Building Information Modelling) methodology to build a digital twin of an old stone pavement road using point clouds obtained from laser scanners and enrichments its semantics. The workflow realised the reverse engineering of existing linear infrastructure with geometric and non-geometric information, which can assist the infrastructure's conservation, maintenance, and restoration.

Secondly, some studies focus on planning and design, and in these studies, a DT can be built for the existing road and surroundings to assist in urban or rural planning. Jiang, et al. [29] proposed a DT-MCDM-GIS (Digital Twin- Multi-Criteria Decision Making-Geographic Information System) framework to assist in sustainable urban road alignment selection for both new road construction and existing road widening considering various factors. Several DT-based methods were proposed for various factors such as building demolition, land use, and traffic congestion. `Dembski, et al. [12] developed a city DT comprising a street network model using the theory and method of space syntax, a 3D model of the built environment, an urban mobility simulation, a wind flow

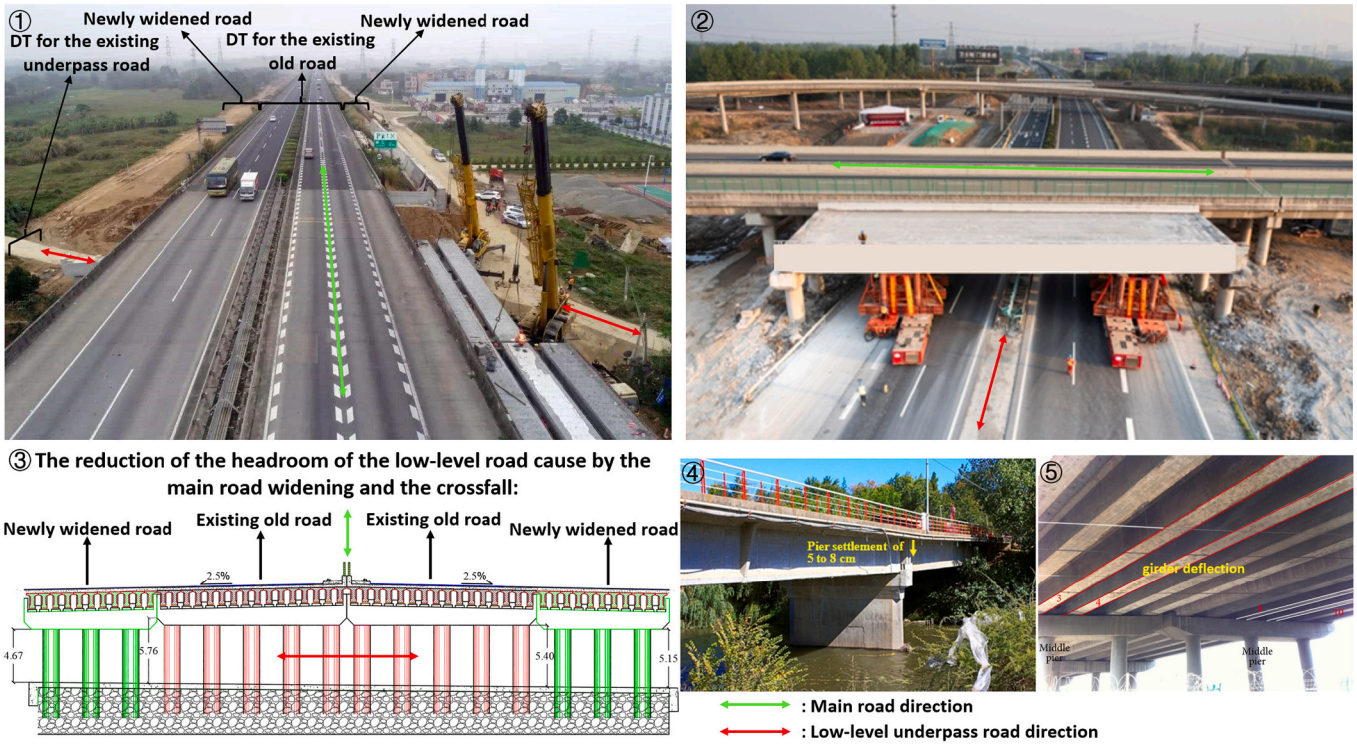

Fig. 1. Clearance reduction of low-level underpass roads in main road widening projects [43,56].

simulation, and many empirical quantitative and qualitative data using volunteered geographic information to assist urban planning. Taniguchi, et al. [46] employed photogrammetry to build a DT for the 3D geometry of the existing walking space by collecting photographic images taken on sidewalks. The method could provide first-person views of the ground and accurate geolocation of the barriers on the map by leveraging a web-based data visualisation tool in GIS to assist walking navigation. Machl, et al. [36] presented digital methods for supporting planners in designing agricultural core road networks based on the DT of the cultivated landscape.

Thirdly, some studies focus on traffic operation. Since roads are the foundation of the traffic flow, road digital twin can be built to assist traffic-related research. Broekman, et al. [6] developed a mini edge artificial intelligence platform for real-time edge processing based on the DT of a multi-lane freeway. The platform could count vehicles together and estimate the speed of each detected vehicle accurately. Charissis, et al. [8] developed a full-scale virtual reality driving simulator that immersed the drivers in challenging, collision-prone scenarios within a DT model. Wang, et al. [51] proposed the automatic traffic modelling method by capturing the sensor data of real-world traffic and replicating the DT version of the traffic condition surrounding the autonomous vehicles to test autonomous vehicles with the captured real traffic in the simulated environment. Tihanyi, et al. [47] developed a working functional prototype of a cooperative perception system that maintained a DT of the traffic environment.

Fourthly, other studies focus on road maintenance based on the digital twin of the existing old road. Yu, et al. [57] proposed a performance prediction approach for highway tunnel pavement based on a digital twin, multiple time series stacking (MTSS) and machine learning. The method was applied in highway pavement life cycle management and achieved accurate results compared to the existing dataset of pavement performance. Ye, et al. [55] conducted a visual inspection, operational monitoring, forced excitation testing, controlled load testing, non-destructive probes, long-term monitoring, finite element modelling, parameter identification, and DT development for a 30-year-old expressway bridge in New Jersey, which helps to determine the root causes of multiple complex performance defects systematically. Kaewunruen, et al. [32] presented digital twin applications of a bridge, including model establishment, information collection and sharing, data processing, inspection, and maintenance planning which could become a more effective information platform for all stakeholders to mitigate risks and uncertainties of exposure to extreme weather conditions over the entire life cycle. Steyn and Broekman [45] developed a DT for a local road network that integrates data from unmanned aerial vehicles and traffic counting artificial intelligence photogrammetric reconstruction technique based on a proprietary neural network environmental condition sensors and commercial temperature sensors. The combination of advanced environmental monitoring data, physical data, and surface temperature data based on the DT could provide management data that could assist in the maintenance of roads. Oreto, et al. [39] presented an efficient and automatic BIM-based life cycle assessment (LCA) method to integrate various environmental factors to assist road pavement design and sustainable pavement maintenance.

2.2. Check and guarantee the highway clearance

Sufficient clearance is vital to the safety of highway structures and vehicles, but clearance can be reduced due to some reasons. Cerullo, et al. [7] addressed an accident on a bridge that was damaged when a dump truck violated the height clearance limitation on the highway. The collision caused extensive damage to the precast/prestressed bridge girders, which led to the closure of the two-lane bridge. Yazdani and Montero [54] reported a bridge damaged from the over-height vehicles due to the existing underpass road remaining open and the temporary vertical lower clearance than the final design during the construction of the overpass bridge. Sometimes, long vehicles with low clearances could be stranded when attempting to pass rail–highway crossings with steeply graded profiles—hump crossings due to the combination of grade profile and cross-section interacting with unique vehicle dimensions. Thus, Liu, et al. [35] proposed a 3D LiDAR-based methodology to identify and evaluate the severity of hump crossings. A five-level criterion was proposed to rate the magnitude of contact, which could provide a good predicted degree of vehicle-crossing conflicts compared to those observed in the field and the method applied to operations (e.g., truck routing) or maintenance and reconstruction programs. In addition, the periodic variation of the water level under the highway structures can reduce the clearance. Jilun, et al. [30] analysed the bridge clearance and ship collision probability on different parts of the arch ring of an arch bridge at different water levels to deduce the annual collapse frequency of the grand bridge.

Several methods were proposed to check the clearance of highway bridges and underpasses by using LiDAR, laser scanner, strain gauge, other sensors, cameras, and GIS. Birge [5] developed a system to determine road stations and the offsets and elevations of visible objects in two photos by taking photolog pictures from a vehicle running on the highway. In this way, bridge clearance, degree of curve, and skew distances can be determined accordingly. Osegueda, et al. [40] developed an automated program for routing overweight vehicles with load-carrying and vertical clearance restrictions for bridges in a road network using a network routing procedure in a GIS platform. The program could automatically identify all bridges on a specified route and evaluate the adequacy of the bridge structures and vertical and horizontal clearance requirements for a given vehicle. Horberry, et al. [24] experimented with a new design of markings for low bridges. They built a full-size bridge capable of having its overhead clearance adjusted. Subjects sat in a truck cab as it drove towards the bridge and were asked to judge whether the vehicle could pass safely under the bridge. Based on the theory of kinematic survey, Gräfe [19] developed a Mobile Road Mapping System equipped with cameras and laser scanners to reconstruct digital road surface models. The system could obtain 360° profiles to assist in analysing bridge clearances and kinematic tunnel surveys. Watson, et al. [52] employed ground-based and vehicle-mount terrestrial LIDAR scanners to recreate the bridge point clouds to measure the bridge clearance. They monitored the bridge periodically to determine the effects of ambient overhead vehicle crossing and seasonal temperature variation on clearance measurements. Gargoum, et al. [18] proposed an algorithm to check the clearance of overhead objects on highways using mobile LiDAR data, which could detect and classify all overhead objects on a highway segment. The clearance was then assessed at each of those objects, and minimum clearance could be identified. Jeon and Lee [26] proposed a method of estimating the displacement of girder bridges constructed at the site by using measured strain signal induced by vehicular loads and the analytically derived strain-displacement relationship where it is difficult to install a fixed reference point for its measurement. The method could be employed to estimate the displacement and clearance of girder bridges that cross rivers, highways and railways.

Several measures relating to highway clearance were proposed. Halliday [22] suggested designing and constructing a highly skewed motorway bridge on a restricted site where the road had an acute intersection angle and limited clearance. Consequently, the structure had a high skew and a thin slab deck, and a haunched slab was chosen as the best solution to the requirement of limited clearance between the local roading and the motorway over the bridge. Hite, et al. [23] presented a program to elevate major highway bridges using very short columns referred to as steel pedestals to address the issue of limited vertical clearance heights and reduce the likelihood of impact damage from the height vehicle collisions. Dehnert and Prevedouros [17] modelled four low-clearance underpasses along a congested arterial. They found that low-clearance underpasses could reduce traffic congestion at intersections where other alternatives have been exhausted, and low-clearance underpasses would be significantly less

expensive than standard underpasses. Sharma, et al. [44] developed a bridge bumper that could reduce the physical injuries and the likelihood of fatalities caused by the collision between the low clearance bridge and vehicles and protect the structural elements of bridges by absorbing the impact energy. Ozdagli, et al. [41] analysed the effectiveness of crash beams for impact attenuation of over height vehicle collisions on railroad bridges to compare three types of crash beams.

2.3. Research gaps from the literature review

From the literature review, several research gaps can be found:

1. All the research measured the highway clearance through field surveys. No study used online map data to check the highway clearance preliminarily.
2. No study proposed a systematic method for road widening based on DT, which should be ideal for solving highway widening-related problems.

3. Methodology

3.1. Data processing and alignment fitting

Since a road is controlled by its horizontal alignments, vertical alignments, and cross-sections, first and foremost, alignments should be fitted based on the limited data from the online map database. In this research, data from aerial photographs, digital surface model (DSM), and digital terrain model (DTM) were downloaded from Digimap [13]. The overall workflow is shown in Fig. 2.

First, the pixels of road markings are extracted from the aerial photographs. The workflow can be expressed by ①-③ in Fig. 3. To make the road markings more apparent, the brightness and contrast of the aerial photograph should be adjusted appropriately using Eqs. (1)–(2), where (i,j) denotes the position of a pixel in the aerial photograph. i, j are integers, and $0 \le i \le m$, $0 \le j \le n$ (② in Fig. 3). The position of a pixel (i,j) is counted from the upper-left (northwest) corner to the bottom-right (southeast) corner of the photograph, and m and n determine the size of the aerial photograph. Thus, the position of the pixel on the aerial photograph at the bottom-right (southeast) corner can be expressed by (m,n). $Old_{R,G,B}(i,j)$ and $New_{R,G,B}(i,j)$ denote the original R, G or B values (red, green, blue) of a pixel and the new R, G, B values of a pixel after digital image processing, respectively. b and c denote the adjusted value of the brightness and the adjusted contrast value, respectively. In Eqs. (1)–(2), $New_{R,G,B}(i,j)$ and $Old_{R,G,B}(i,j)$ are integers, and $0 \le New_{R,G,B}(i,j), Old_{R,G,B}(i,j) \le 255$. The value range of b and c are [0,1]. b and c should be given appropriate values according to the colours of the aerial photograph. After the brightness and contrast of the aerial photograph are adjusted, its Y, U, V values should be calculated according to its R, G, B values by Eqs. (3)–(5), where Y, U, V are integers and their ranges are [0,255], [−127,128], and [−127,128], respectively. i, j denote the position of a pixel in the aerial photograph. The YUV model defines a colour space in terms of one luma component (Y) and two chrominance components, called U (blue projection) and V (red projection), respectively. Y represents the brightness of a pixel. The U and V samples represent the colour deviations towards blue and red [53]. After that, the characters of the pixels of road markings should be analysed, and their pixels should be extracted according to their characters (③ in Fig. 3). Generally, the road markings are brighter than in other areas, which means that the $Y(i,j)$ is no smaller than an appropriate threshold (T_1). In addition, road markings are whiter than in other areas, which means the differences between the R, G, B values of a pixel are not large, and $U(i,j)$ and $V(i,j)$ should be no larger than appropriate thresholds (T_2) and (T_3), as shown in Eq. (6).

There are also some shadows on the pavement caused by the trees, vehicles, and facilities. In shadows, the brightness of road markings can be lower than that of other areas with no shadows. However, the road markings are locally brighter than the surrounding areas representing the road pavement. Thus, another condition should be proposed to extract the road marking pixels, as shown in Fig. 4. First, the direction of the shadow should be determined. For each aerial photograph, different parts were shot approximately in the same period when the directions of the sun were similar, and the directions of the shadow were roughly the same. For any line segment (red line segment in Fig. 4) parallel to the shadow direction, the ratio of the Y-direction increment to the X-direction increment represents the direction of the shadow. The positive direction of X is east, and the positive direction of Y is south. After that, for each pixel (target pixel), starting from its left and right sides, select k pixels (nearby pixel) from near to far on each side. Including the target pixel and the selected k pixels on the left and right, respectively, $2k+1$ pixels are arranged in a straight line. The direction of the straight line should be roughly the same as the direction of the shadow. However, if the direction of the road is approximately parallel to the direction of the shadow, the straight line should not be parallel to the direction of the shadow and should be roughly perpendicular to the road direction. If the target pixel is the pixel on the road markings, its brightness should be much larger than the average brightness of the $2k+1$ pixels. Thus, Eqs. (7) and (8) express another condition to select the pixels of the road markings, where *Round* denotes the rounded value towards the nearest integer, *abs* denotes the absolute value, and X and Y represent the increment of the line segment parallel to the shadow direction at X-direction and Y-direction, respectively, and k are integers. Thus, for the selected $2k+1$ pixels, if $abs(Y) \ge abs(X)$, the ratio of the i increment to the j increment is the rounded value towards the nearest integer of the ratio of Y to X. It is similar if $abs(Y) < abs(X)$. p is a proportional parameter which should be given an appropriate value according to how brighter the road marking pixels are than the other pixels in the selected surrounding $2k+1$ pixels. Thus, the pixels of road markings can be extracted by conditions in Eqs. (6)–(8) and appropriate parameters T_1, T_2, T_3, and p. After that, according to the relationship between the pixels and the coordinates of the centres of the pixels in the real world, the pixels can be converted into the coordinate points called road marking points (RMPs) (④ in Fig. 3).

$$New_{R,G,B}(ij) = \left(Old_{R,G,B}(ij) - 127.5 \times (1-b)\right) \bullet k + 127.5 \times (1+b) \quad (1)$$

$$k = tan((45+44c)/180 \bullet \pi) \quad (2)$$

$$Y(i,j) = 0.299R(i,j) + 0.587G(i,j) + 0.144B(i,j) \quad (3)$$

$$U(i,j) = -0.169R(i,j) - 0.331G(i,j) + 0.5B(i,j) \quad (4)$$

$$V(i,j) = 0.5R(i,j) - 0.419G(i,j) - 0.081B(i,j) \quad (5)$$

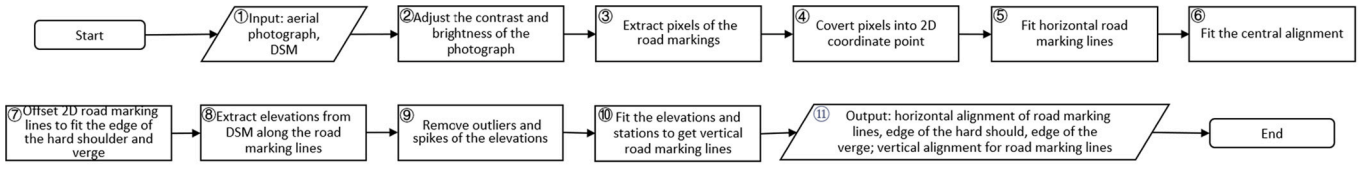

Fig. 2. Workflow for horizontal and vertical alignment fitting.

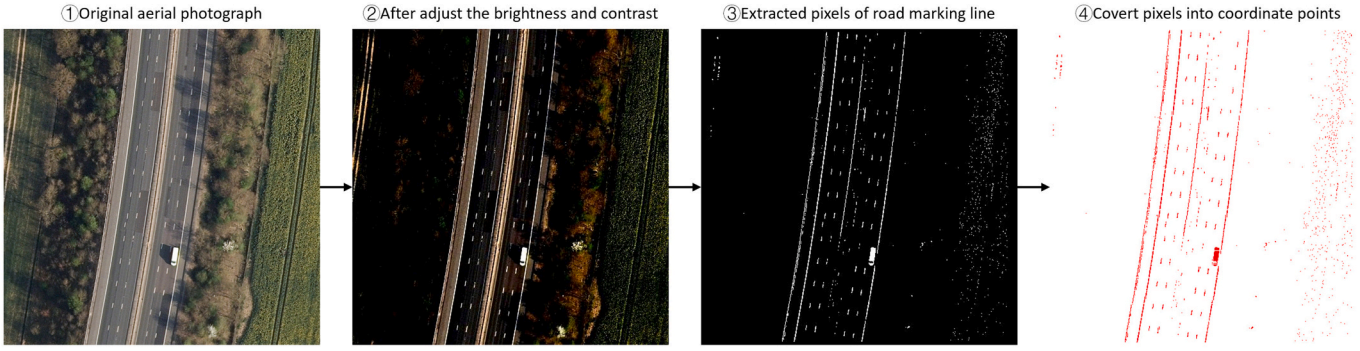

Fig. 3. Road marking pixels extraction.

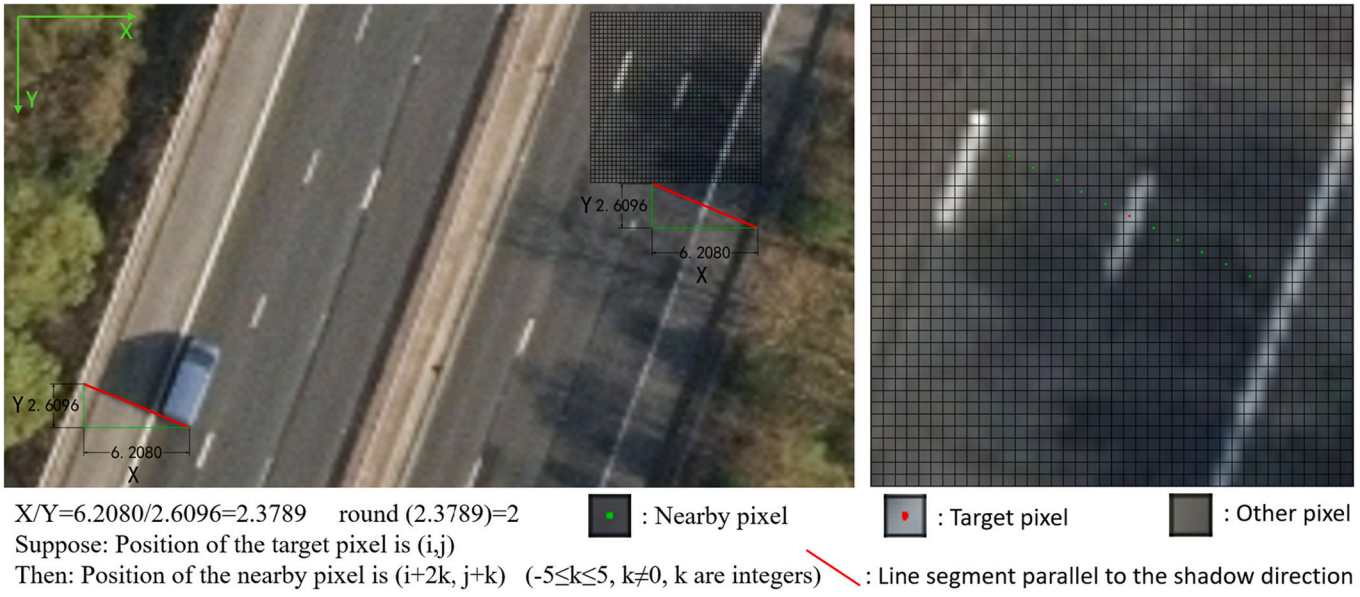

Fig. 4. Condition for extracting road marking pixels.

$$Y(i,j) \geq T_1, U(i,j) \leq T_2, V(i,j) \leq T_3 \tag{6}$$

$$Y(i,j) \geq p \times \sum_{k=-5}^{5} Y(i+k \bullet Round(Y/X), j+k) \Big/ 11, (if\ abs(Y) \geq abs(X)\ ) \tag{7}$$

$$Y(i,j) \geq p \times \sum_{k=-5}^{5} Y(i+k, j+k \bullet Round(X/Y)) \Big/ 11, (if\ abs(Y) < abs(X)\ ) \tag{8}$$

After the coordinate points of the road markings are obtained, smoothing splines are employed to fit the road markings using the coordinate points, as shown in Eq. (9). In the equation, f is the function of the smoothing spline, which is a twice-differentiable function on [a,b]. The smoothing spline strives to find the smallest value of $S(f)$. λ is the smoothing parameter defined on [0,1]. When $\lambda = 0$, a least-squares straight-line fitting to the data can be obtained. When $\lambda = 1$, a cubic spline interpolant going through all the data points can be generated [37]. The smoothing splines will fit the overall trend, and the local data missing has little effect on the overall fit. Thus, T_1, T_2, T_3, and p in Eqs. (6)–(8) can take values within a suitable range rather than strictly specific values. The general principle is "less is better than wrong", which means T_1, T_2, T_3, and p can be set more severe to extract fewer road marking points rather than keeping outliers. Eqs. (10) and (11) can interpret the quality of the fitting result. RMSE (root mean square error) is the square root of the second sample moment of the differences between predicted values and observed values which can evaluate the overall deviation between the smoothing spline and original points. $R-square$ (coefficient of determination) is a statistical measure representing the proportion of the variance for a dependent variable explained by an independent variable or variables in a regression model. Usually, the larger the $R-square$ is, the better the regression model fits the data.

The smoothing spline fitting the coordinate points of the road markings are called horizontal road marking lines (HRML), as shown in Fig. 5. After that, the central horizontal alignment (CHA) should be fitted, as shown in ① in Fig. 5. Since the road marking points (RMPs) are missing in some areas on one side and exit on the other side, the CHA should not be fitted using the RMPs directly. Otherwise, the CHA can fluctuate. Thus, after the HRML4 and HRML5 are fitted, their points are extracted per meter along the X-axis or along the Y-axis. Then, the CHA can be fitted based on the extracted points by a smoothing spline. After that, the elevations on the cross-section of the original road along the CHA by stations can be extracted from DSM. Since the slope of the side slope is significantly larger than the slope of the pavement and verge, the slope of the cross-section has a mutation on the edge between the verge and the side slope. Thus, the edge line between the verge and the side slope (horizontal verge line (HVL)) can be determined by offsetting the HRML1 and HRML8 by a specific value according to the mutation position, as shown in ② in Fig. 5. For the edge line between the hard

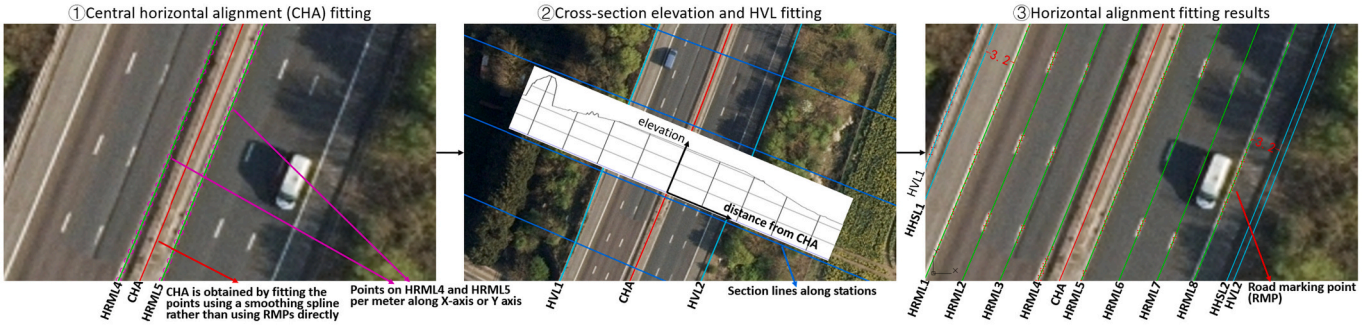

Fig. 5. Horizontal alignment fitting.

shoulder and verge (horizontal hard shoulder lines (HHSL)), the offset values can be determined by the design standards [15]. For example, according to standards for highways in the UK, as shown in Fig. 6 [15], a lane road marking line is just between two adjacent lanes, but the edge road marking lines are totally on the hard shoulder or hard strip. Generally, the width of a lane road marking line is 0.15 m, and the width of an edge road marking line is 0.2 m. The width of a hard shoulder is 3.3 m. Thus, HRML1 and HRML8 are offset (3.3–0.2/2) = 3.2 m outwards to represent the HHSL1 and HHSL2, respectively, as shown in ③ in Fig. 5.

$$S(f) = \lambda \sum_{i=1}^{n} (y_i - f(x_i))^2 + (1-\lambda) \int_a^b (f''(x))^2 dx \tag{9}$$

$$RMSE = \sqrt{\sum_{i=1}^{m} (y_i - \hat{y}_i)^2 \Big/ m} \tag{10}$$

$$R - square = \sum_{i=1}^{m} (\hat{y}_i - \bar{y}_i)^2 \Big/ \sum_{i=1}^{m} (y_i - \bar{y}_i)^2 \tag{11}$$

The alignment fitting method is the same for the existing low-level underpass road. There are not as many components as the main road, which are much easier to be fitted, as shown in Fig. 7. After HRMLs are fitted, other important edges can be fitted by offsetting the HRMLs. Some existing low-level underpass roads do not have a central reserve, and a road marking is drawn in the middle of the pavement. For this circumstance, the CHA does not need to be fitted by the extracted points from two adjacent HRMLs. Instead, the CHA can be fitted directly by the RMPs in the middle of the pavement.

After horizontal alignments are fitted, elevations along HRMLs of the main road are extracted from the DSM, as shown in ① in Fig. 8. Thus, the original elevations from DSM and the corresponding stations (the accumulated mileage from the start point along the horizontal alignment) of an HRML can be obtained, as shown in ② in Fig. 8. Since there are some spikes and outliers on the pavement caused by defects on the pavements, vehicles, guardrails, poor data quality, etc., the Hampel filter is employed to remove the spikes and outliers of the original elevations from the DSM, as shown in ③ in Fig. 8. Eqs. (12)–(15) can interpret the Hample filter process, where x_i represent the original elevations from the DSM, y_i are the filtered results, n and t should be given appropriate values. The Hampel filter employed n elevation values before x_i and n elevation values after x_i to evaluate if x_i can be regarded as an outlier or spike. If $|x_i - m_i| > tS_i$, x_i should be regarded as an outlier or spike and should be replaced by m_i. Preferably, the value given to n should ensure the W_i^n can include more data than the longest continuous outliers or spikes. For example, the longest continuous outliers or spikes are produced by long vehicles. If the estimated length of a long vehicle is 8 m, and the elevations are extracted per 0.2 m along the HRML, the n can be assigned a value of 25 ($0.2 \times 25^*2 = 10 > 8$). The smaller t, the greater the probability that x_i will become an outlier or spike. After that, a smoothing spline is employed to fit the elevations after the Hampel filter process and their corresponding stations according to Eq. (9), as shown in ④ in Fig. 8. Only the HRMLs are employed to extract elevations on the DSM, and the obtained smoothing splines fitting the elevations after the Hampel filter process are called vertical road marking lines (VRMLs).

$$W_i^n = \{x_{i-n}, \ldots, x_i, \ldots, x_{i+n}\} \tag{12}$$

$$m_i = median\{x_{i-n}, \ldots, x_i, \ldots, x_{i+n}\} \tag{13}$$

$$y_i = \begin{cases} x_i & |x_i - m_i| \le tS_i \\ m_i & |x_i - m_i| > tS_i \end{cases} \tag{14}$$

$$S_i = 1.4826 \times median_{j \in [-n,n]} \{|x_{i-j} - m_i|\} \tag{15}$$

Existing road data are on the DSM. Though DTM can filter some buildings and trees in DSM, existing roads can also be embodied on DTM. In two circumstances, DSM and DTM should not be used directly. One is establishing the DT model of existing road and road widening, and the other is extracting elevations along the HRMLs of the current

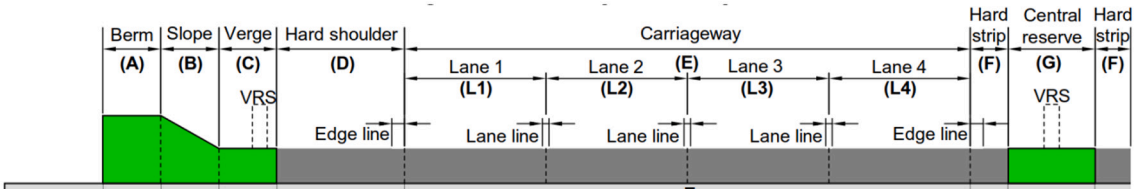

Road type	A	B	C	D	E				F	G
					L1	L2	L3	L4		
Dual 2 lane (D2M)	Varies	Varies	1.50	3.30	7.30				0.70	3.10
					3.65	3.65	N/A			
Dual 3 lane (D3M)	Varies	Varies	1.50	3.30	11.00				0.70	3.10
					3.65	3.70	3.65	N/A		
Dual 4 lane (D4M)	Varies	Varies	1.50	3.30	14.70				0.70	3.10
					3.65	3.70	3.70	3.65		

Fig. 6. Dimensions of standard cross-sections from the design standard.

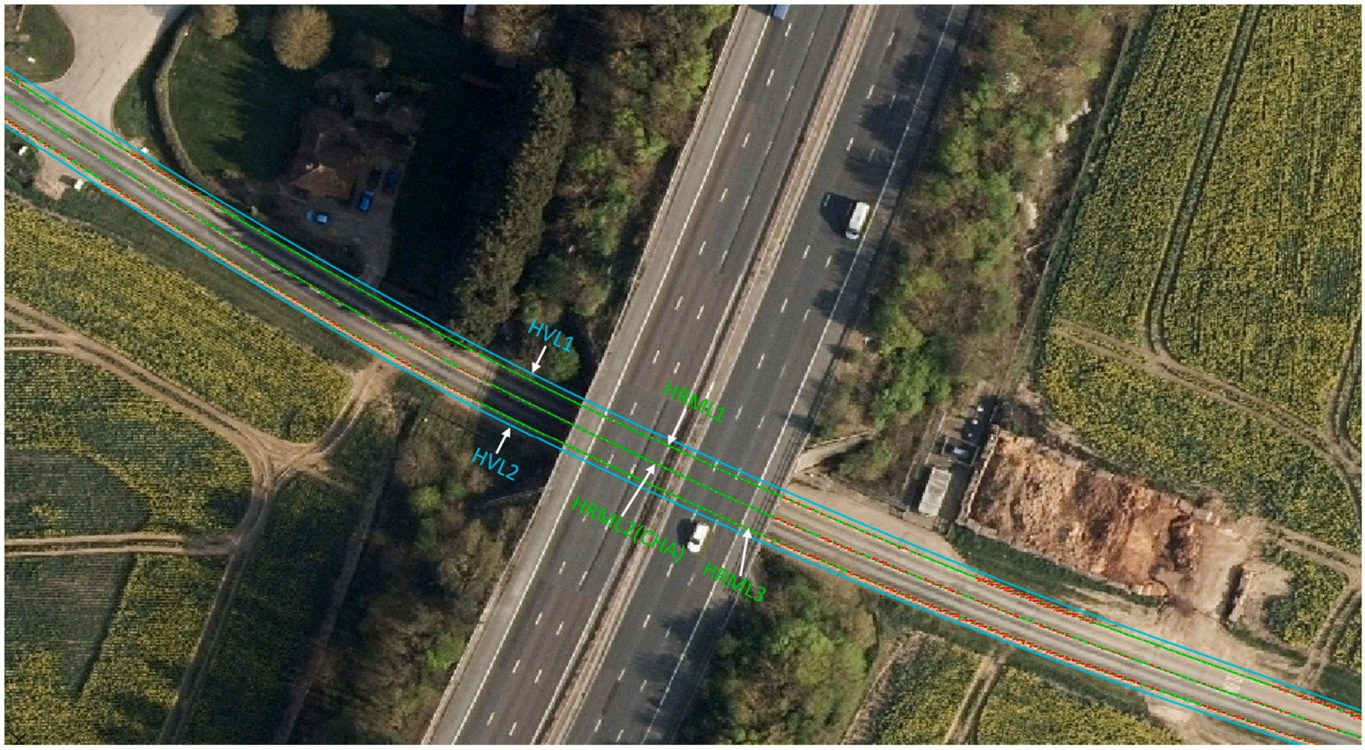

Fig. 7. Horizontal alignment fitting of the existing low-level underpass road.

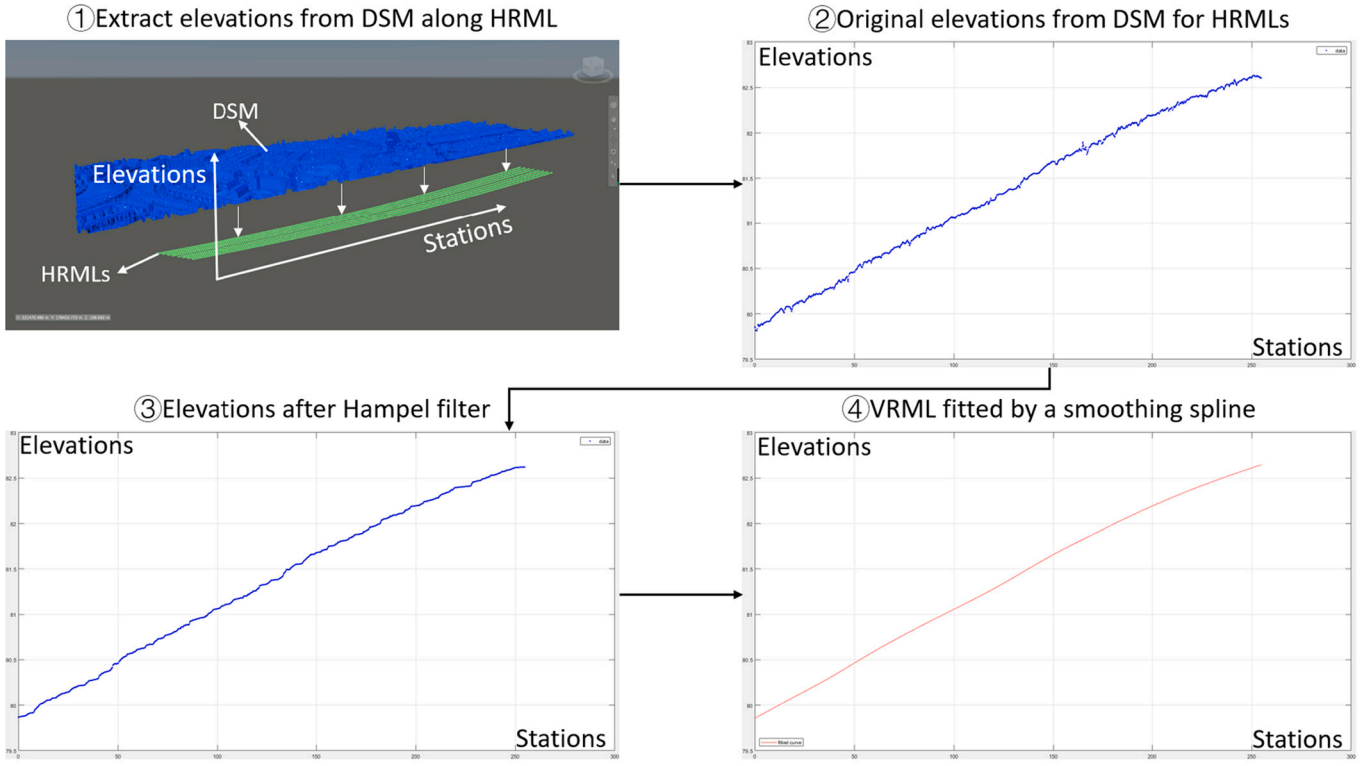

Fig. 8. Generation of vertical road marking lines (VRML).

low-level underpass road. In the first circumstance (①–⑧ in Fig. 9), the existing road is constructed based on the original natural terrain (⑨ and ⑩ in Fig. 9) rather than the surface of the built road. Thus, if DSM is employed to develop the digital model, in some areas, the pavement can be buried into the DSM and can get the wrong side slope intersecting with the existing slope or outliers on the existing slope on the DSM. Though some outliers of the DSM are removed on DTM, similar problems still exist when DTM is employed for modelling. In the second circumstance (⑪ and ⑫ in Fig. 9), when extracting the elevations of the existing low-level underpass road directly from DSM, the extracted

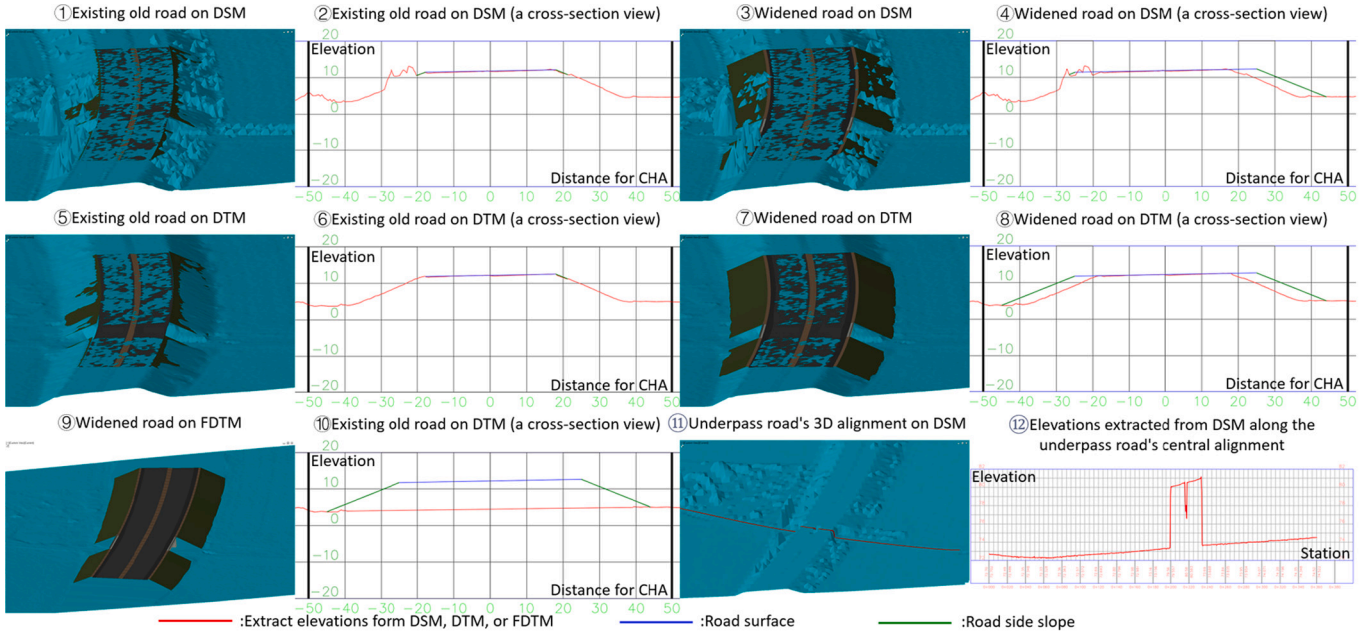

Fig. 9. Problems of using DSM or DTM directly.

elevations at the underpass areas are the elevation of the existing main road. Thus, the elevations along the existing low-level underpass road will rise and fall dramatically in the underpass area. Therefore, DSM and DTM should be processed for data extraction and road modelling, called flattened DSM (FDSM) and flattened DTM (FDTM), and the process is shown in Fig. 10.

First, the slopes of DTM are calculated, and the raster representing the slopes' values is established (② in Fig. 10). Second, in the raster representing the slope values, the data remain unchanged if the slopes are >10%, and the data in other areas will be deleted to form no data areas (③ in Fig. 10). Third, the points from the rasters in ③ in Fig. 10 are extracted as shown in ④ in Fig. 10. Fourth, a TIN (Triangulated Irregular Network) is established using the extracted points, and the maximum triangle side length should be limited by T_4 (⑤ in Fig. 10) [17]. If the precision of the downloaded original DTM is 0.5 m (side length of the square cell), the maximum triangle side length should be set to a number that is $>0.5\sqrt{2}$ considering the differences of z values. For example, T_4 can be set to one. Fifth, the boundary of the TIN can be extracted, and

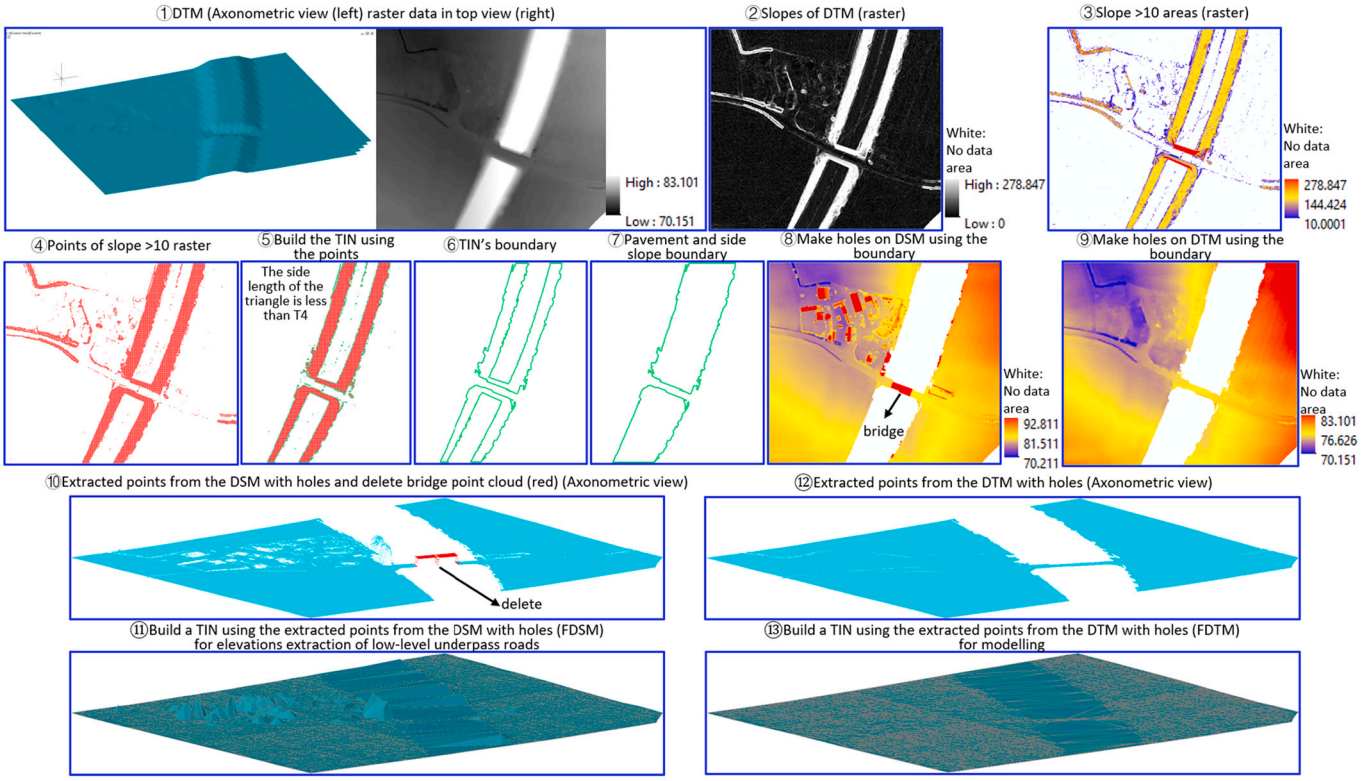

Fig. 10. Establishment of flattened DSM (FDSM) and flattened DTM (FDTM).

the boundaries of the road's side slopes can be obtained (⑥ in Fig. 10). Sixth, the outer boundaries of the road's side slopes can be combined into the boundaries of the road (⑦ in Fig. 10). Seventh, in the area of the road's boundaries, the data are removed on the DSM and DTM to form no-data areas (holes) (⑧ and ⑨ in Fig. 10). Eighth, the point of the DSM with holes and DTM with holes are extracted (⑩ and ⑫ in Fig. 10). The bridge point clouds should be deleted on the DSM. Finally, two new TINs will be built using the extracted points without bridge point clouds from the DSM with holes or DTM with holes to represent flattened DSM (FDSM) and flattened DTM (FDTM). The irregular triangles are still built in the no-data areas of DSM with holes and DTM with holes. FDSM will be employed to extract elevations along the horizontal alignment of the existing low-level underpass road. After that, the extracted elevations should be filtered by Hampel filter and fitted by smoothing splines to represent the vertical road marking lines (VRMLs), as shown in Fig. 11. FDTM will be employed to model. For all alignment elevation extractions, DSM (for the main road) or FDSM (for the existing low-level underpass roads) should be employed rather than DTM or FDTM, because DSM and FDSM can reflect the actual elevations of the road surface.

3.2. Road digital twin and road widening model

Following the previous step, the DT of the existing main road and existing low-level underpass road and the model of the newly widened road can be established with the control of the horizontal alignments and the vertical alignments. Horizontal alignments include central horizontal alignment (CHA), horizontal road marking lines (HRMLs), horizontal hard shoulder lines (HHSLs), and horizontal verge lines (HVLs). Vertical alignments are vertical road marking lines (VRMLs).

First of all, one of the most critical things in this section is to establish assemblies of the cross-sections with appropriate suitable constraints. This section takes the widening of a two-way six-lane road into a two-way eight-lane road as an example to explain the method. For the DT of the existing main road, two sections should be considered: road and bridge sections, as shown in Fig. 12. Thus, two types of assemblies should be established. First, the assembly should consider the central reserve, hard strips, lanes, hard shoulders, verges, and side slopes in the road sections. Then, based on the road sections, the assembly of the bridge cross-sections is established, and the bridge model can be built.

Second, several constraints can be set to control the assembly of the cross-sections. In Fig. 12, P (control point), H (horizontal line), and V (vertical line) denote the control points of the assemblies, horizontal lines that control the horizontal positions of the control points, and vertical lines that control the elevations of the control points, respectively.

Third, the relationships between P, H, and V should be determined. There are two categories of control points. In the first category, control points can be determined only by the horizontal lines (H) and vertical lines (V) directly, such as P3 to P10, as shown in Fig. 12. Control points in the second category should be determined by the control points in the first category. The line connecting P3 and P9 is named L1, and the line connecting P4 and P10 is named L2. P1, P11, and P13 are the intersections of L1 with H1, H11, and H13, respectively. P2, P12, and P14 are the intersections of L2 with H2, H12, and H14, respectively. P0 is the intersection of the line connecting P1 and P2 with H0. P15 and P16 are the intersections of the side slopes with the FDTM. The side slopes can be determined by P13, P14 and the specific slope of the side slopes.

Fourth, the cross-sections of the road and bridge can be determined. The cross-sections should consider the thickness of the pavement and the bridge superstructure. HRMLs, HHSLs, HVLs, and CHA can determine the positions of horizontal lines (H), VRMLs can determine the vertical lines (V).

Finally, the DT of the existing main road can be established by sweeping the cross-sections along with the CHA, considering the constraints from horizontal lines (H) and vertical lines (V). There are road sections from Station 1 to Station 3 and from Station 4 to Station 6. From Station 3 to Station 4, there is a bridge section. Since the elevations of VRMLs change independently, the values of the cross fall and superelevations can be generated automatically.

Based on the DT of the existing main road, the BIM model of the widened road can be established, as shown in Fig. 13. P15 and P17 are the intersections of L1 with H15 and H17, respectively. P16 and P18 are the intersections of L2 with H16 and H18, respectively. P19 and P20 are the intersections of the side slopes with the FDTM. The side slopes can be determined by P17, P18 and the specific slope of the side slopes. The road components between P14 and P13 are the digital twin parts of the existing road. The road components between P20 & P14 and P13 & P19 are the BIM models of the newly widened road. The components between P14 & P12 and P11 & P13 are the old verges of the existing road, which will be constructed into the new pavement in the widened road.

The DT of the existing low-level underpass road is similar to but much easier than the main road. The model development method is the same, but fewer components are involved. This section takes low-grade roads without central reserve as an example, as shown in Fig. 14. P0, P1, and P2 are directly controlled by horizontal lines (H) and vertical lines (V). The line connecting P0 and P1 is named L1, and the connecting P0 and P2 is named L2. P3 is the intersection of L1 and H3, and P2 is the intersection of L2 and H4. HRMLs and VRMLs determine horizontal (H) and vertical (V) lines. P5 and P6 are the intersections of the side slopes with the FDTM. The side slopes can be determined by P3, P4 and the specific slope of the side slopes.

3.3. Clearance check and redesign of the underpass road

After establishing the digital models of the widened main road and existing low-level underpass road, the models are placed in the correct coordinate system. Then, the surface of the existing low-level underpass road is extruded upwards vertically by a specific value (the designed clearance according to the design standard) to form a 3D model, which is named as Road Clearance Model (RCM) (① in Fig. 15). Afterwards, clash

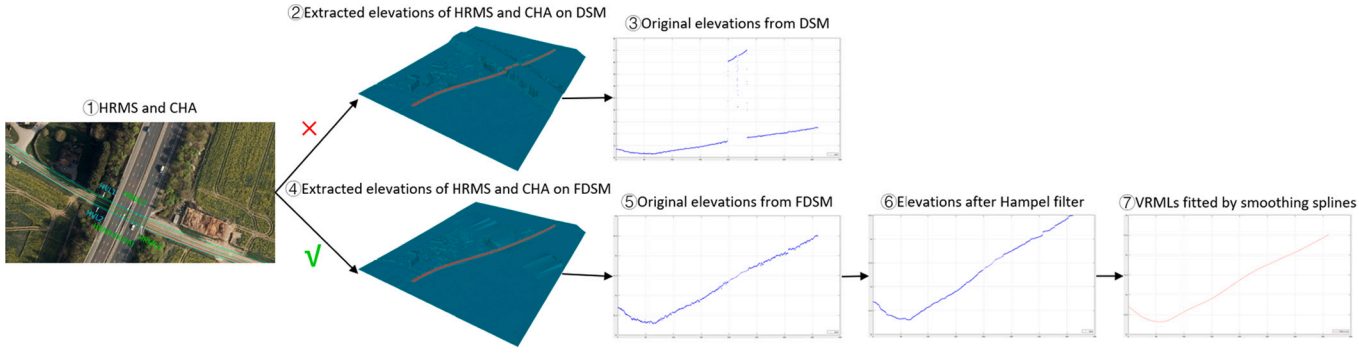

Fig. 11. Vertical alignment fitting for the existing low-level underpass road using FDSM.

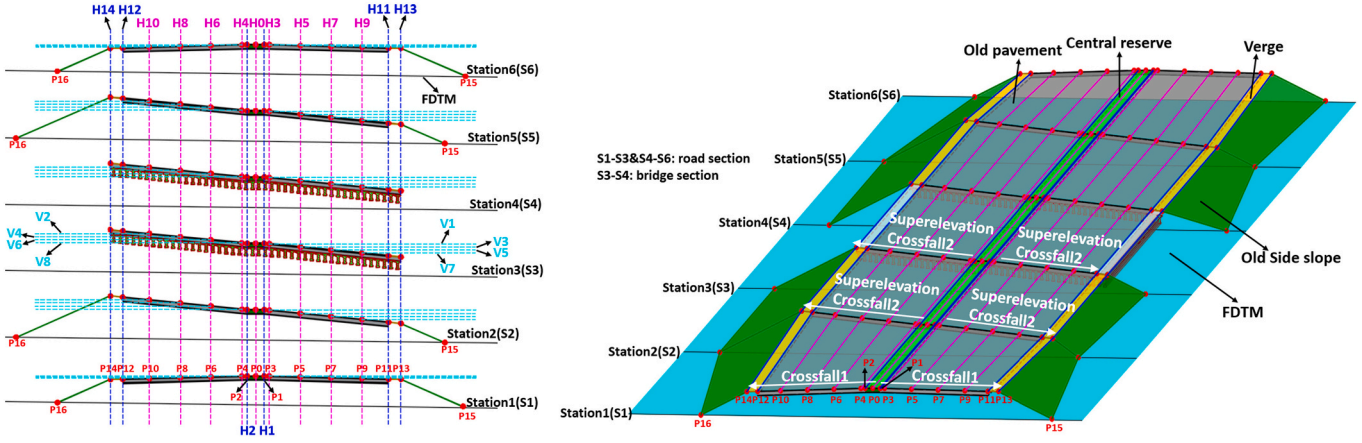

Fig. 12. Digital twin of the existing main road.

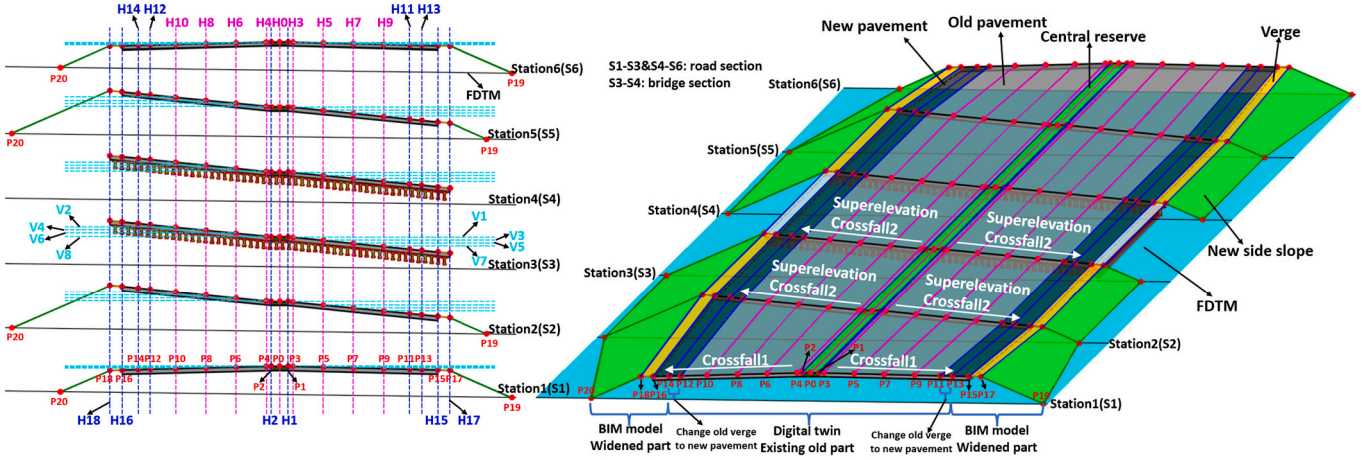

Fig. 13. BIM model of the newly widened road based on the digital twin of the existing main road.

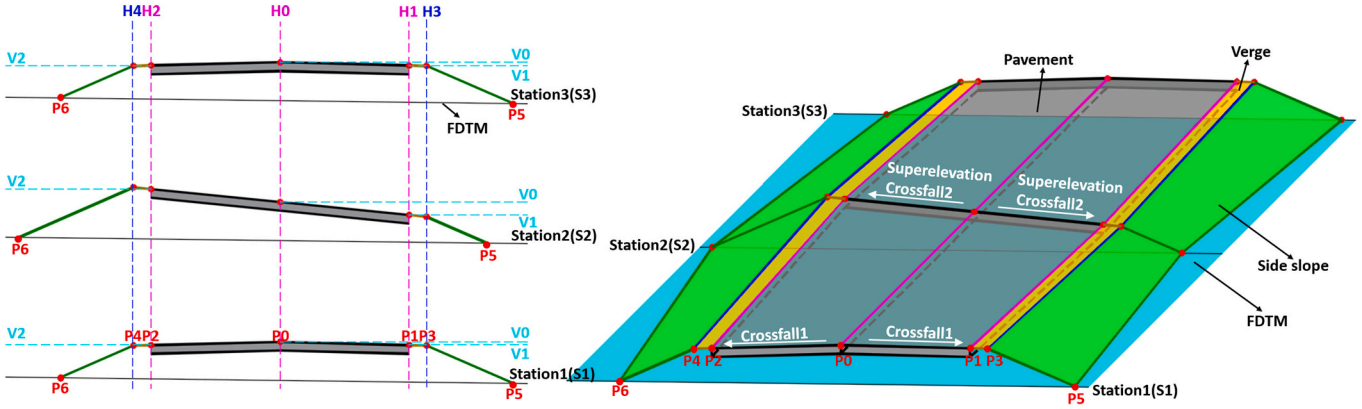

Fig. 14. Digital twin of the existing low-level underpass road.

detection is performed between the widened main road and the RCM (② in Fig. 15). Without clashes, the existing low-level underpass road clearance can meet the requirement after widening the main road. If any clash exists, the clearance of the existing low-level underpass road cannot meet the requirement after widening the main road, and the existing low-level underpass road should be redesigned and constructed, as shown in Fig. 16. The intersection parts of the RCM with every widened road component which has a clash with the RCM can be extracted to facilitate the redesign process. After that, the whole intersection parts are projected into 2D drawings on the profile view of the existing low-level underpass road. Then the projected 2D drawing of the intersection part is moved down by the required clearance value. Accordingly, the vertical alignment (VRML2 (the vertical road marking line of HRML2 in Fig. 7)) of the low-level underpass road should be redesigned to ensure the new profile is lower than the moved 2D drawing of the intersection. In addition, other VRMLs should be adjusted

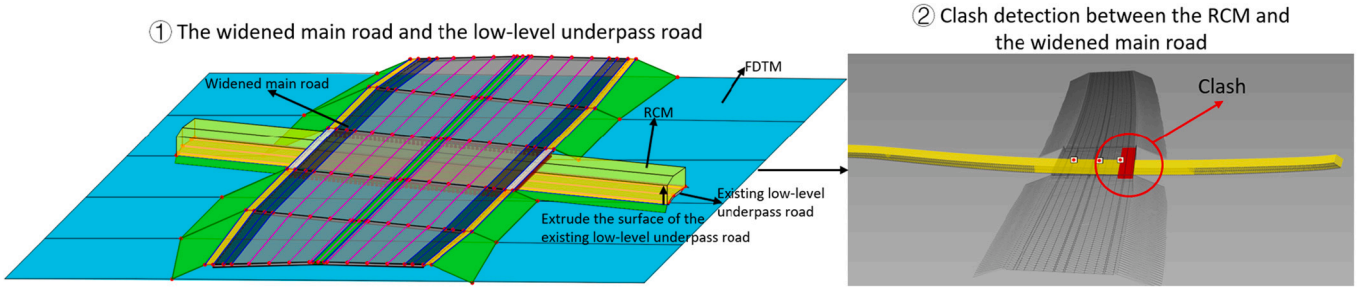

Fig. 15. Clearance check of the existing low-level underpass road.

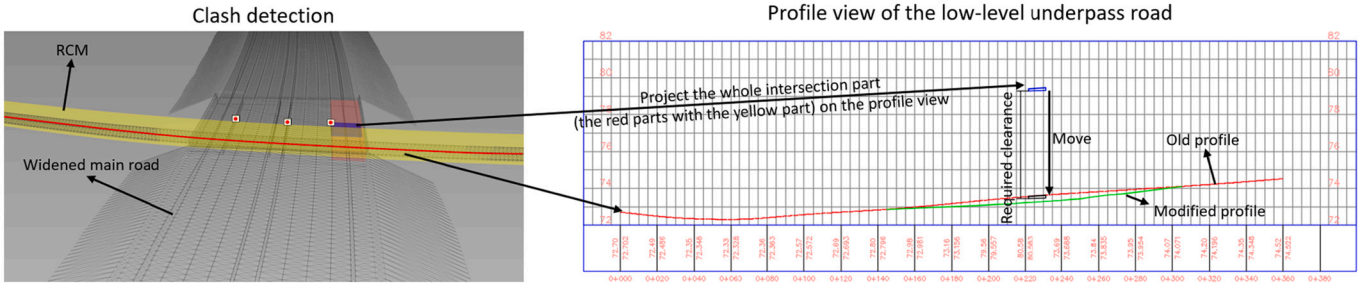

Fig. 16. Redesign of the existing low-level underpass road.

according to the redesigned vertical alignment.

4. Case study

The M11 motorway is a two-way six-lane motorway. The selected low-level underpass road is Sawbridgeworth Road, a two-way two-lane road. The underpass is located in the northern part of Epping Forest District, Essex County, UK, and its coordinate are (51° 48′ 52.8834″°N, 0° 10′ 58.6092″E), as shown in Fig. 17. The DSM, DTM, and aerial photograph data were downloaded from Digimap [13,14]. The proposed method was mainly implemented in MATLAB R2020b. ArcGIS10.3 was employed to process DSM and DTM data, Civil 3d 2021 assisted in the road modelling process, and Navisworks Manage 2021 was used for clash detection.

Data of the DSM, DTM, FDSM, and FDTM is shown in Fig. 18. The continuous area with slopes larger than 10% in DTM was employed to extract the area of the existing road to make no-data areas on the DSM and DTM. The precision of the downloaded DSM and DTM is 0.5 m; thus, the value of T_4 is assigned 1 to limit the side length of the reconstructed TIN (⑤ in Fig. 10). The parameters for road marking extraction are shown in Table 1, and the original aerial photograph and the road marking extraction process are shown in Fig. 19. The meaning of the parameters is expressed in Eqs. (1)–(8). There is much dirt on the existing underpass road, so the road is yellowish. Thus, U's absolute value is large, and T_2 is not employed to limit the U value in the road marking point extraction process of the underpass road. Since the lanes

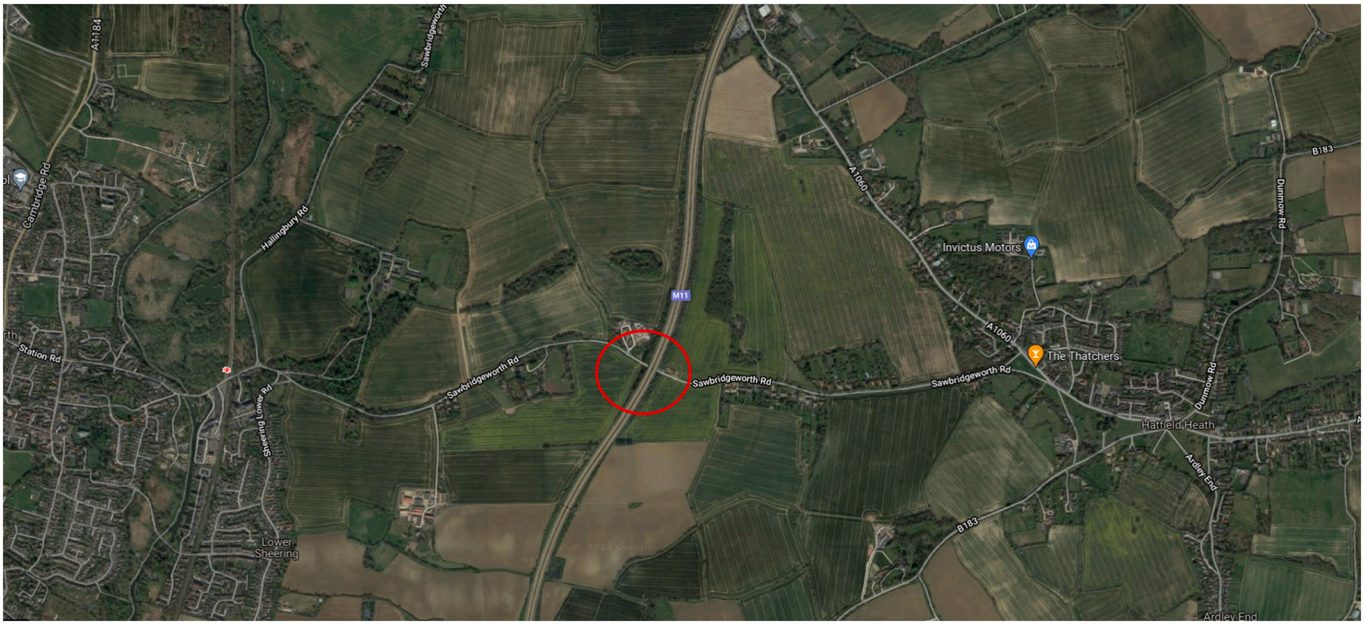

Fig. 17. Location of the target roads in Goole Maps.

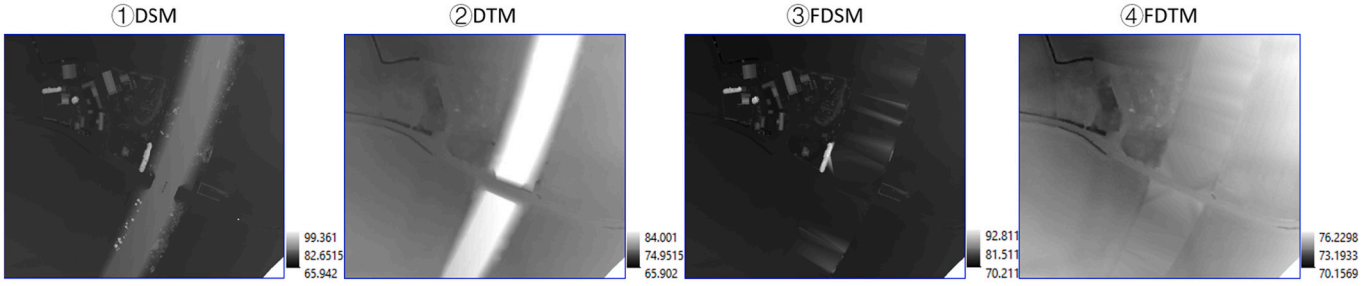

Fig. 18. Original and flattened DSM, DTM data.

Table 1
Related parameters for road marking point extraction.

Roads	Brightness & contrast adjustment		Road marking pixel Extraction					
	b	c	T_1	T_2	T_3	p	k	Round
Main road	−0.1	0.5	127	15	15	1.5	5	3 (X/Y)
Underpass road	−0.2	0.5	127	–	25	2	3	2 (Y/X)

of the main road are wider than the lanes of the underpass road, and there are some bright strips caused by dirt on the pavement of the underpass road, the k value for the underpass road is smaller than that for the main road.

The horizontal alignment fitting results and corresponding parameters are shown in Table 2, Fig. 20, and Fig. 21. HHSL1 and HHSL2 can be obtained by offsetting HRML1 and HRML2 outwards by 3.2 m. HVL1 and HVL2 can be obtained according to the aerial photograph and mutations of the cross-section lines extracted from DSM. The fitting results of VRMLs for HRMLs are shown in Table 3 and Fig. 22. The original elevation of the VRMLs of the existing main road and the underpass road are extracted from the DSM and the FDSM, respectively. The HVL3 and HVL4 can be obtained by offsetting HRML9 and HRML11 by 0.1 m outwards.

According to the existing documents of the target projects and design standards, the thickness of the main road pavement is 0.355 m [49], and the thickness of the newly designed bridge deck, including the asphalt concrete pavement and the waterproofing system, is 0.2 m [16]. The bridge span is 30.159 m from the station number of K0 + 031.430 to K0 + 061.589, and the designed height of the girders of the bridge superstructure is 1.5 m. The thickness of the underpass road pavement is 0.335 m, which would not influence the clearance checking result in this case study. In addition, the side slopes of the underpass road are not considered. Thus, the cross-sections of the widened main road and the existing low-level underpass road are shown in Fig. 23. The relationships for modelling are expressed in Table 4. The DT of the existing road and the low-level underpass road, and the model of the widened main road are shown in Fig. 24.

The designed deflection of the bridge was estimated at 30.159/800, and the required clearance was 5.30 + 30.159/800 = 5.338 m [15]. Thus, the RCM can be obtained by extruding the underpass road surface upwards by 5.338 m. The clearance check is completed by referring to the clash detection results between the widened main road and the RCM, as shown in Fig. 25. The intersection (clearance intersection (CI)) between the widened road and the RCM can be obtained by the Boolean operation on the 3D solids. The CI can be projected on the profile view of the underpass road. According to the clearance check, the clearance is not enough if the existing main road employs the newly designed bridge. On the left side of the main road, road widening reduces the clearance significantly. On the right side of the main road, though the vertical alignment of the underpass road rises, the widened road still can meet the clearance requirement. The reason is that there is a superelevation in this section of the main road, and the right part of the main road is higher than the left part of the main road. According to the moved CI, the underpass road's vertical alignment (VRML10) should be redesigned to increase the insufficient clearance, as shown in Fig. 26.

The BIM model for the redesigned underpass road was established according to the redesigned vertical alignment, as shown in Fig. 27. From K0 + 000.000 to K0 + 063.272 and K0 + 342.840 to K0 + 350.000, Cross-section 1 will be used for modelling. It is the same as the cross-section for the underpass road DT. The V0 of Cross-section 1 follows the redesigned vertical alignment, and other constraints (H0 to H4, V1, and V2) still follow the relationships in Table 4. However, the redesigned vertical alignment in these two sections is the same as the VRML10. Thus, the BIM model remains the same as the DT of the underpass road. From K0 + 083.272 to K0 + 302.840, Cross-section 2 will be used for modelling, in which H0 to H4 also follow the relationships in Table 4 and V0 follows the redesigned vertical alignment. However, there are no V1 and V2 to control the elevations of P1 and P2, and the

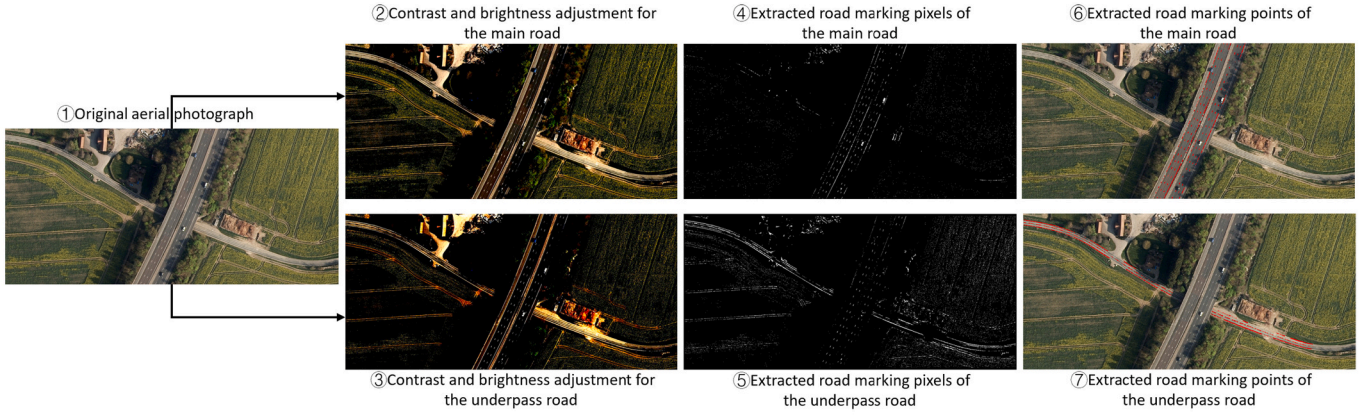

Fig. 19. Road marking extraction for the main road and underpass road.

Table 2
Results and parameters of the horizontal alignment fitting.

Station	HRML1		HRML2		HRML3		HRML4		HRML5	
	x	y	x	y	x	y	x	y	x	y
K0 + 000	550,540.919	215,085.563	550,544.072	215,084.078	550,547.471	215,082.478	550,550.738	215,080.940	550,554.795	215,079.031
K0 + 020	550,549.423	215,103.664	550,552.673	215,102.134	550,555.976	215,100.580	550,559.266	215,099.031	550,563.210	215,097.173
K0 + 040	550,557.650	215,121.893	550,560.961	215,120.336	550,564.291	215,118.769	550,567.541	215,117.238	550,571.402	215,115.417
K0 + 060	550,565.650	215,140.224	550,568.954	215,138.669	550,572.305	215,137.093	550,575.635	215,135.527	550,579.476	215,133.715
K0 + 080	550,573.427	215,158.650	550,576.824	215,157.056	550,580.153	215,155.489	550,583.498	215,153.916	550,587.293	215,152.123
K0 + 100	550,581.052	215,177.139	550,584.375	215,175.574	550,587.725	215,173.999	550,590.931	215,172.483	550,594.835	215,170.647
K0 + 120	550,588.300	215,195.778	550,591.565	215,194.237	550,594.940	215,192.652	550,598.082	215,191.161	550,602.151	215,189.260
K0 + 134	550,593.160	215,208.908	550,596.472	215,207.349	550,599.814	215,205.776	550,602.972	215,204.279	550,607.012	215,202.389
λ	6.572E-4		6.572E-4		6.572E-4		2.419E-4		2.131E-2	
RMSE	0.09644		0.1053		0.1167		0.1338		0.07846	
R-square	1.0000		1.0000		1.0000		0.9999		1.0000	

Station	HRML6		HRML7		HRML8		CHA		HHSL1	
	x	y	x	y	x	y	x	y	x	y
K0 + 000	550,557.972	215,077.535	550,561.324	215,075.957	550,564.601	215,074.414	550,552.735	215,080.000	550,538.031	215,086.922
K0 + 020	550,566.500	215,095.625	550,569.855	215,094.046	550,573.153	215,092.494	550,561.193	215,098.124	550,546.537	215,105.022
K0 + 040	550,574.794	215,113.824	550,578.133	215,112.252	550,581.489	215,110.673	550,569.474	215,116.328	550,554.800	215,123.236
K0 + 060	550,582.835	215,132.136	550,586.218	215,130.545	550,589.487	215,129.004	550,577.529	215,134.635	550,562.770	215,141.579
K0 + 080	550,590.623	215,150.558	550,594.003	215,148.967	550,597.285	215,147.421	550,585.317	215,153.056	550,570.546	215,160.005
K0 + 100	550,598.173	215,169.078	550,601.524	215,167.499	550,604.858	215,165.932	550,592.823	215,171.593	550,578.147	215,178.504
K0 + 120	550,605.434	215,187.713	550,608.758	215,186.145	550,612.083	215,184.581	550,600.094	215,190.225	550,585.400	215,197.142
K0 + 134	550,610.344	215,200.823	550,613.656	215,199.260	550,616.960	215,197.704	550,605.097	215,203.300	550,590.266	215,210.270
λ	2.419E-4		6.572E-4		2.419E-4		3.742E-6			
RMSE	0.1151		0.09539		0.1124		2.3922			
R-square	1.0000		1.000		1.000		0.9850			

Station	HHSL2		HVL1		HVL2	
	x	y	x	y	x	y
K0 + 000	550,567.533	215,073.034	550,536.787	215,087.508	550,568.133	215,072.752
K0 + 020	550,576.061	215,091.125	550,545.612	215,105.455	550,576.661	215,090.842
K0 + 040	550,584.390	215,109.308	550,554.352	215,123.442	550,584.764	215,109.121
K0 + 060	550,592.392	215,127.637	550,562.353	215,141.771	550,592.887	215,127.390
K0 + 080	550,600.188	215,146.055	550,569.464	215,160.463	550,600.784	215,145.762
K0 + 100	550,607.765	215,164.564	550,576.770	215,179.080	550,608.362	215,164.271
K0 + 120	550,614.988	215,183.214	550,584.076	215,197.698	550,615.586	215,182.921
K0 + 134	550,619.863	215,196.337	550,588.982	215,210.810	550,620.461	215,196.044
λ						
RMSE						
R-square						

Station	HRML9		HRML10		HRML11		HVL3		HVL4	
	x	y	x	y	x	y	x	y	x	y
K0 + 000	550,377.822	215,217.437	550,377.468	215,214.802	550,377.105	215,212.100	550,377.835	215,217.536	550,377.091	215,212.001
K0 + 050	550,426.451	215,206.277	550,426.105	215,203.664	550,425.712	215,200.867	550,426.465	215,206.378	550,425.697	215,200.765
K0 + 100	550,470.443	215,182.771	550,469.883	215,179.744	550,469.315	215,176.650	550,470.460	215,182.878	550,469.297	215,176.543
K0 + 150	550,513.058	215,156.628	550,512.325	215,153.315	550,511.663	215,150.072	550,513.074	215,156.734	550,511.646	215,149.966
K0 + 200	550,557.132	215,133.039	550,556.406	215,129.750	550,555.665	215,126.368	550,557.147	215,133.143	550,555.650	215,126.265
K0 + 250	550,602.747	215,112.581	550,602.006	215,109.263	550,601.301	215,105.954	550,602.762	215,112.683	550,601.286	215,105.852
K0 + 300	550,649.455	215,094.760	550,648.719	215,091.450	550,648.047	215,088.234	550,649.469	215,094.862	550,648.032	215,088.133
K0 + 351	550,697.863	215,078.828	550,697.301	215,076.047	550,696.776	215,073.314	550,697.877	215,078.928	550,696.762	215,073.215
λ	2.392E-3		2.256E-3		9.260E-4					
RMSE	0.1753		0.1097		0.1694					
R-square	1.000		1.000		1.000					

fixed cross fall of 2.5% will control the elevations instead. K0 + 063.272 to K0 + 083.272 and K0 + 302.840 to K0 + 342.840 are the transition sections, where Cross-section 2 is used for modelling. The redesign vertical alignment will determine the V0 of Cross-section 2. However, V1 and V2 do not follow the relationship in Table 4. The elevations of V1 and V2 are the linear transition of the elevations of V1 and V2 in the former section and the next section along HRML10. For example, the elevation of V1 is E1 at K0 + 063.272, and the elevation of V1 is E2 at K0 + 083.272. At Station S, between K0 + 063.272 and K0 + 083.272, the height of V1 is E1 + (E2-E1)·(S- K0 + 063.272)/20. In the transition section, H0 to H4 still follow the relationships in Table 4. After establishing the redesigned underpass road BIM model, a new RCM should be generated according to the new BIM model, and the clearance check should be performed between the widened main road and the new RCM, as shown in Fig. 28. The underpass road can meet the clearance requirement after the redesign.

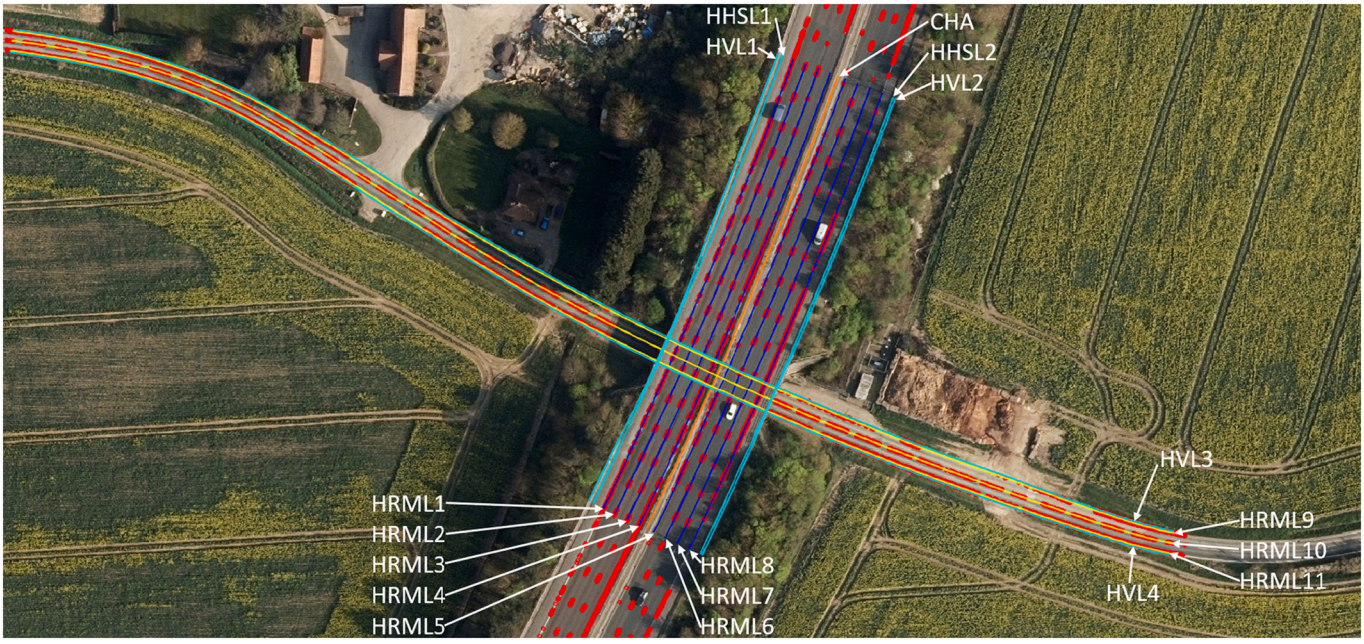

Fig. 20. Positions of horizontal alignments.

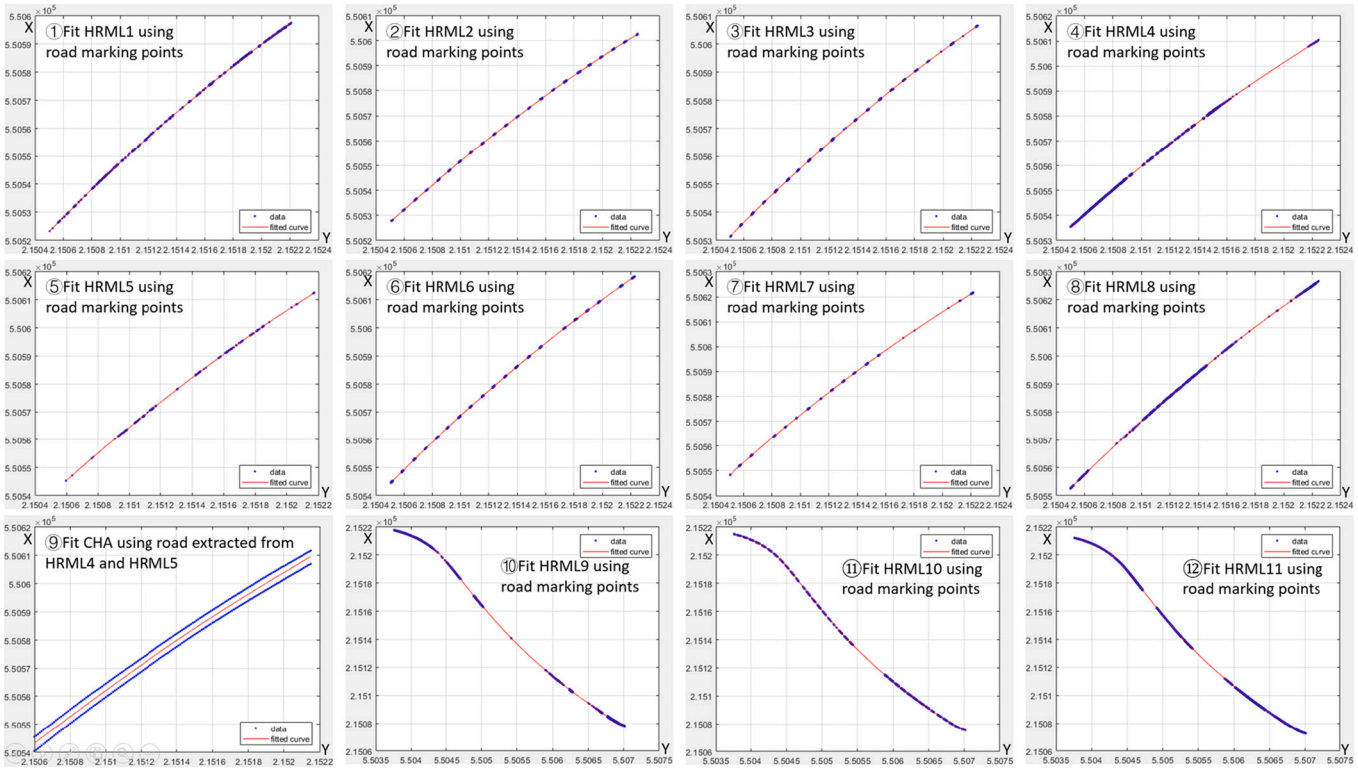

Fig. 21. Fitting results of horizontal alignments.

5. Discussion

The digital twin paradigm can provide a feasible solution to this issue by reconstructing digital replicas for the existing facilities to assist in the renovation, expansion, or reconstruction process. Road widening should be designed and constructed based on the existing roads. However, obtaining all design and construction documents of the existing roads built decades ago is challenging. The data are often too unstructured to be used for making road widening decisions. A DT can reconstruct the model of the existing road using multi-source data by the proposed method, including digital image process, alignment fitting, and cross-section assembly creating to assist in road widening. Based on the DT of the existing road, the digital model of the newly widened road can be built. This research proposes a feasible solution for creating a DT for the existing roads to assist in road widening decisions. Though it is not as accurate as of the field survey data, it is cost-effective in the preliminary

Table 3
Results and parameters of the vertical alignment fitting.

Station	VRML1	VRML2	VRML3	VRML4	VRML5	VRML6
	Elevation (E)	Elevation (E)	Elevation (E)	Elevation (E)	Elevation (E)	Elevation (E)
K0 + 000	79.514347	79.634580	79.766957	79.864581	79.919822	80.036569
K0 + 020	79.774980	79.889866	80.021559	80.132467	80.210659	80.306743
K0 + 040	80.037780	80.148772	80.275738	80.396402	80.483627	80.551523
K0 + 060	80.265450	80.388343	80.505302	80.627815	80.712715	80.776854
K0 + 080	80.502625	80.624703	80.741526	80.856431	80.921384	81.018198
K0 + 100	80.795157	80.901166	81.020584	81.114735	81.147937	81.274462
K0 + 120	81.085388	81.186347	81.305728	81.390231	81.390901	81.517445
K0 + 134	81.277098	81.377280	81.492441	81.580618	81.558513	81.684555
n	25	25	25	25	25	25
t	0.1	0.1	0.1	0.1	0.1	0.1
λ	1.00E-05	1.00E-05	1.00E-05	1.00E-05	1.00E-05	1.00E-05
RMSE	0.01575	0.01295	0.01466	0.01115	0.01562	0.01182
R-square	0.9990	0.9993	0.9991	0.9995	0.9989	0.9994

Station	VRML7	VRML8	Station	VRML9	VRML10	VRML11
	Elevation (E)	Elevation (E)		Elevation (E)	Elevation (E)	Elevation (E)
K0 + 000	80.156690	80.266073	**K0 + 000**	72.762266	72.708017	72.709274
K0 + 020	80.421269	80.543981	**K0 + 050**	72.372853	72.318626	72.297250
K0 + 040	80.667557	80.788149	**K0 + 100**	72.548484	72.566208	72.550913
K0 + 060	80.894222	81.011345	**K0 + 150**	72.852619	72.891522	72.867307
K0 + 080	81.119840	81.234008	**K0 + 200**	73.300947	73.355761	73.313690
K0 + 100	81.368617	81.482643	**K0 + 250**	73.708884	73.750936	73.704321
K0 + 120	81.599281	81.727408	**K0 + 300**	73.999178	74.058891	73.990912
K0 + 134	81.753915	81.880302	**K0 + 351**	74.386888	74.430416	74.551662
n	25	25	**n**	25	25	25
t	0.1	0.1	**t**	0.1	0.1	0.1
λ	1.00E-05	1.00E-05	**λ**	1.00E-4	1.00E-4	1.00E-4
RMSE	0.01485	0.01332	**RMSE**	0.01061	0.009006	0.01117
R-square	0.9990	0.9992	**R-square**	0.9997	0.9998	0.9997

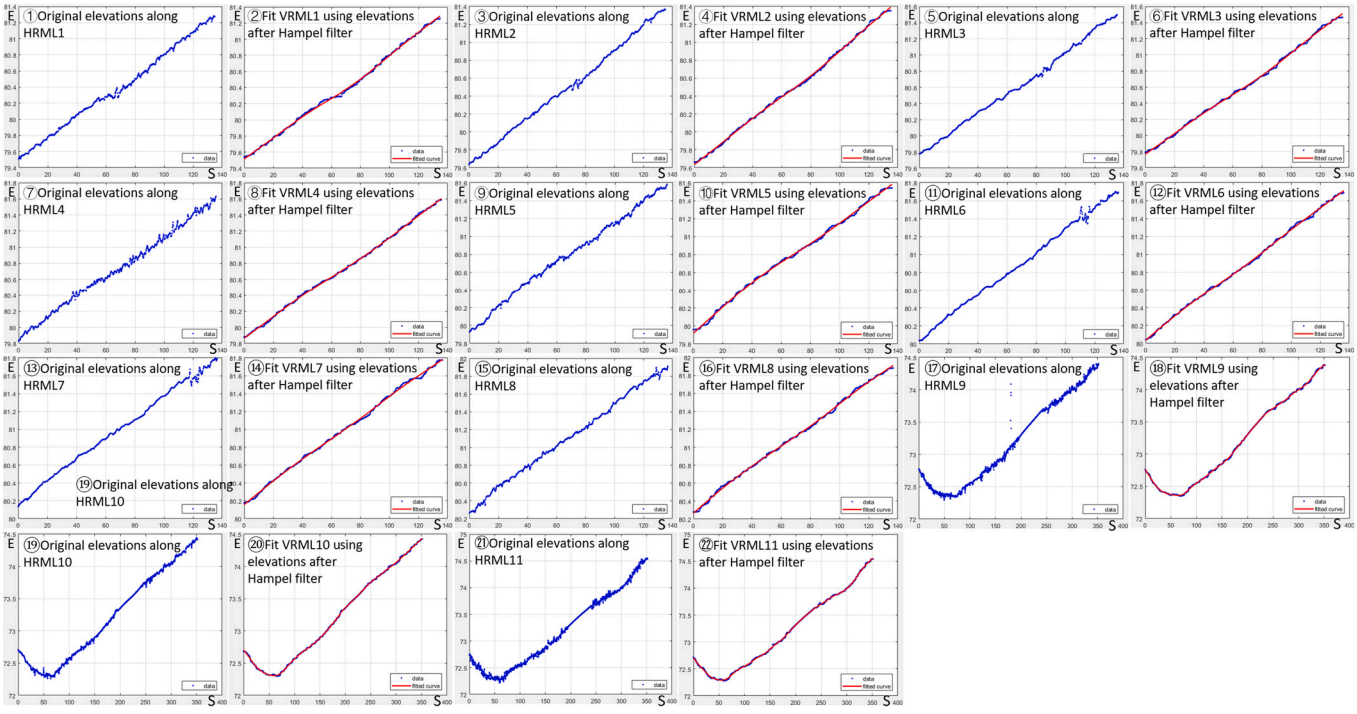

Fig. 22. Fitting results of vertical alignments.

design phase. In addition, if more accurate data can be obtained from field surveys, such as airborne LiDAR surveys, the proposed method can also be employed to build road DT and consider the defects and local inaccuracies of the data.

Road widening projects can significantly influence the surroundings, such as buildings (demolition), land use, existing roads, pipelines, railways, and rivers. Thus, the DT should not only be built for the target road but also should be built for the surroundings. This research focuses

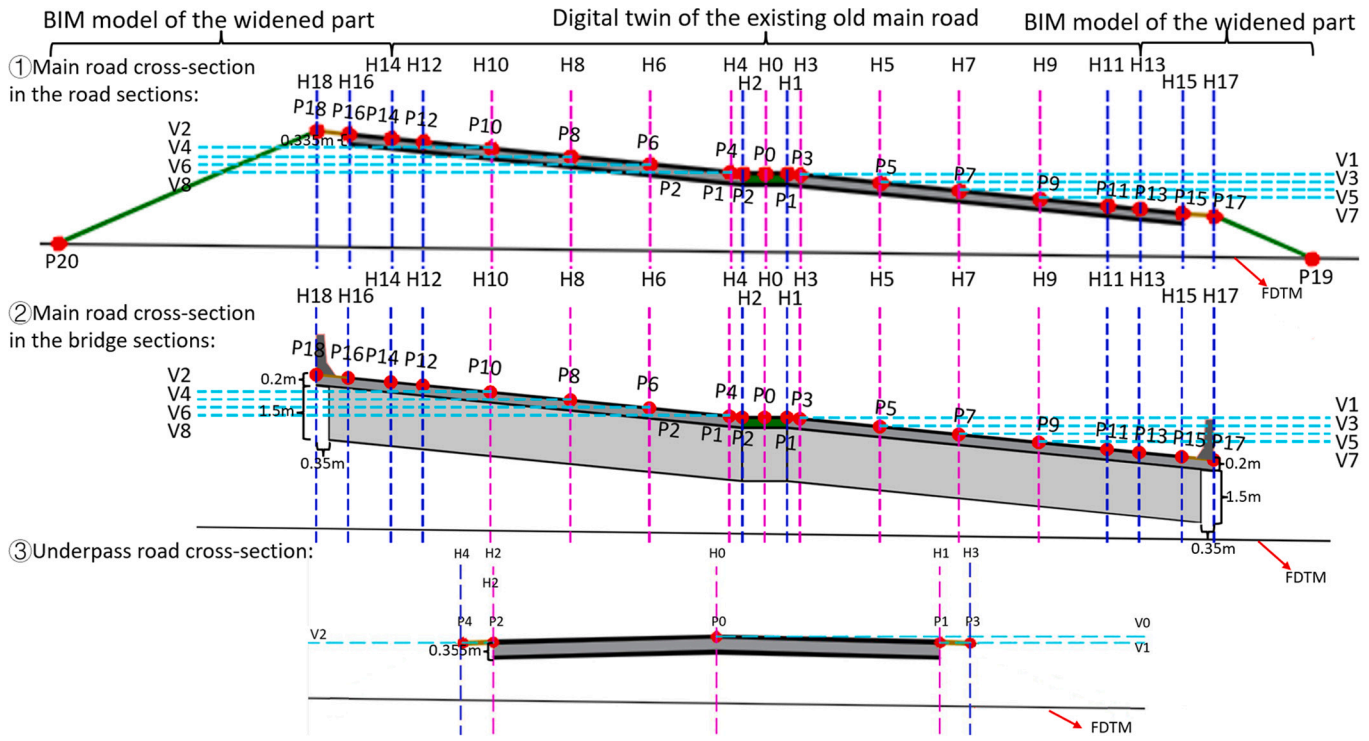

Fig. 23. Cross-sections of the widened main road and the underpass road.

Table 4
Constraints for modelling and their determination methods.

Main road			
Target constraint	Determination method	Target constraint	Determination method
H10	HRML1	H8	HRML2
H6	HRML3	H4	HRML4
H3	HRML5	H5	HRML6
H7	HRML7	H9	HRML8
H0	CHA	H12	HHRL1
H11	HHRL2	H14	HVL1
H13	HVL2	H1	0.7 m to the left of H3
H2	0.7 m to the right of H4	H15	17.9 m to the right of H3
H16	17.9 m to the left of H4	H17	1.5 m to the right of H15
H18	1.5 m to the left of H16	V2	VRML1
V4	VRML2	V6	VRML3
V8	VRML4	V1	VRML5
V3	VRML6	V5	VRML7
V7	VRML8	Side slope value	43.48%
Underpass road			
H2	HRML9	H0	HRHML10
H1	HRML11	H4	HVL3
H3	HVL4	V2	VRML9
V0	VRML10	V1	VRML11

on the influence of road widening on the low-level underpass roads, which are usually ignored in road widening projects. As the explanation in Section 1, the cross fall and road widening of the existing main road, the vertical alignment of the underpass road can reduce the clearance of the underpass road. Thus, in addition to the DT of the existing main road, the model of the low-level underpass road should be built. Clash detection at the design stage can perform the clearance check based on the digital models. Accordingly, the existing low-level road redesign can be conducted to ensure the required clearance. When there are conflicts between a high-level road and a low-level road, the redesign and reconstruction are usually performed on the low-level road to remove the conflict rather than conducted on the high-level road. The proposed method also can be updated and employed for similar projects, such as the reconstruction of the overpass road and road widening of the low-level road.

Furthermore, the existing bridge is usually reconstructed or demolished and rebuilt in the road widening projects, and a new scheme for the underpass bridge is usually proposed according to the newly widened road. In addition, the new bridge is built based on the widened road. Thus, in this research, the proposed method only focuses on the road DT, and the new bridge model after widening can be built based on the newly widened road. The clearance check can be conducted between the models of the newly widened road with the new bridge (the bridge is regarded as a part of the road) and the existing low-level underpass road.

However, there are some limitations of this research. First of all, the accuracy of the proposed method has not been compared with the field survey. To be compared with the field survey, focus groups or interviews are highly suggested to evaluate the proposed method. Secondly, in addition to underpass roads, overpass roads should be considered in future research.

6. Conclusions

This paper described a cost-effective method to build DT for the existing main and low-level underpass roads at the preliminary design stage. First, based on the main road DT, the BIM model of the widened road can be built. Then, according to the widened road BIM model and the underpass road digital twin, the clearance can be checked, and the underpass road can be redesigned.

There are several contributions that this article can bring to the field. First, a systematic digital twin method is proposed for the existing old main road and low-level underpass road based on online map data. In addition, a systematic road widening method is proposed based on the digital twin paradigm. Last but not least, this paper presents a cost-

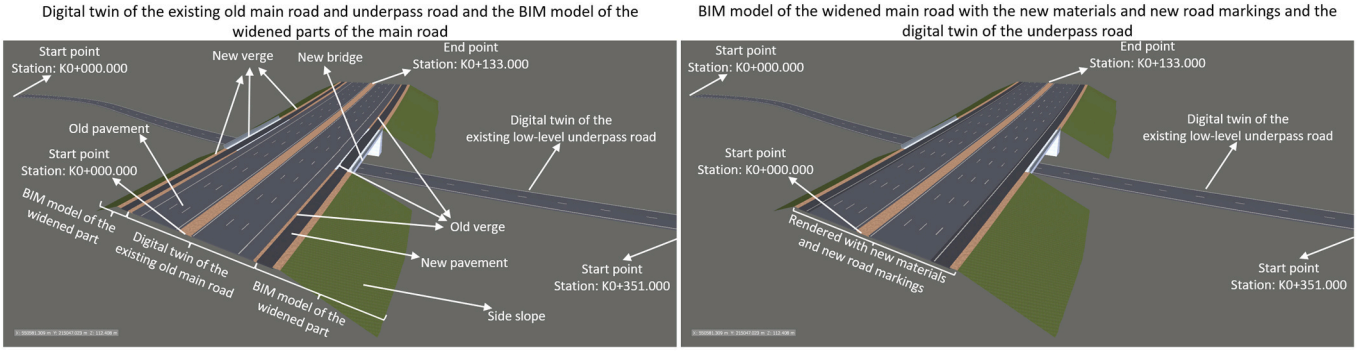

Fig. 24. Digital twins of the existing old main road and underpass road and BIM models of the widened main road.

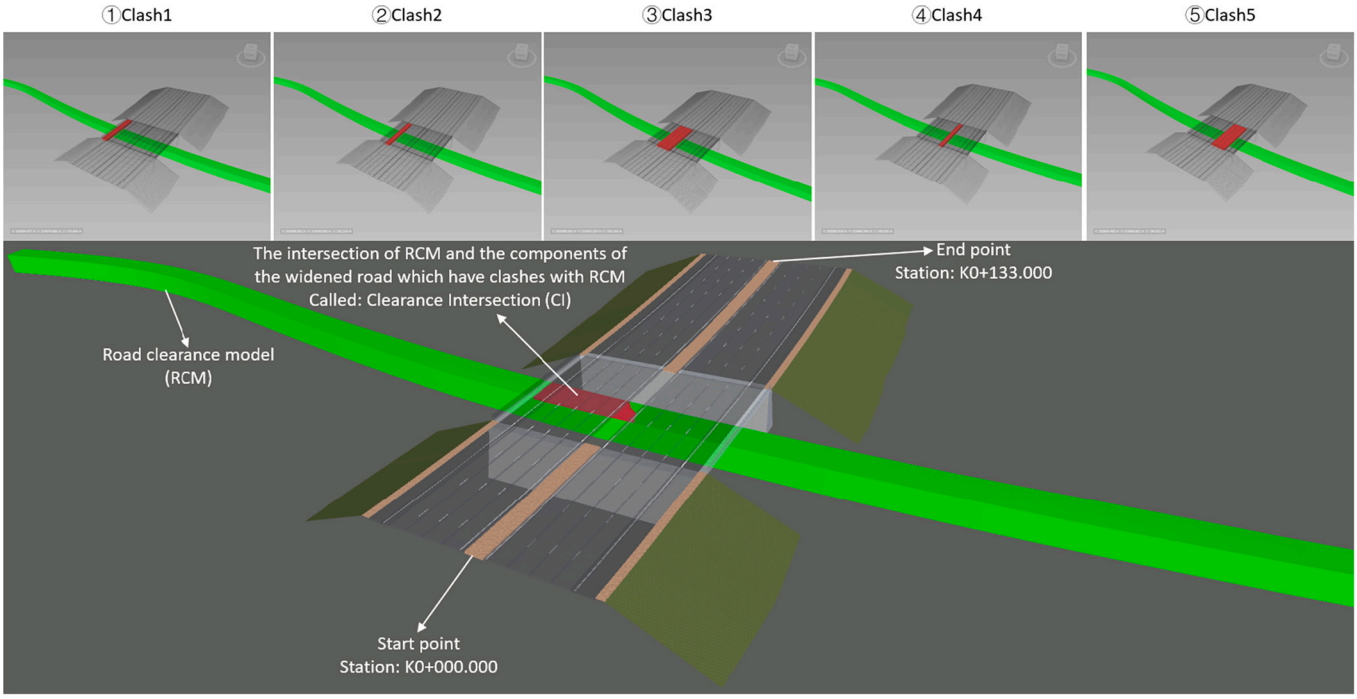

Fig. 25. Clearance check result.

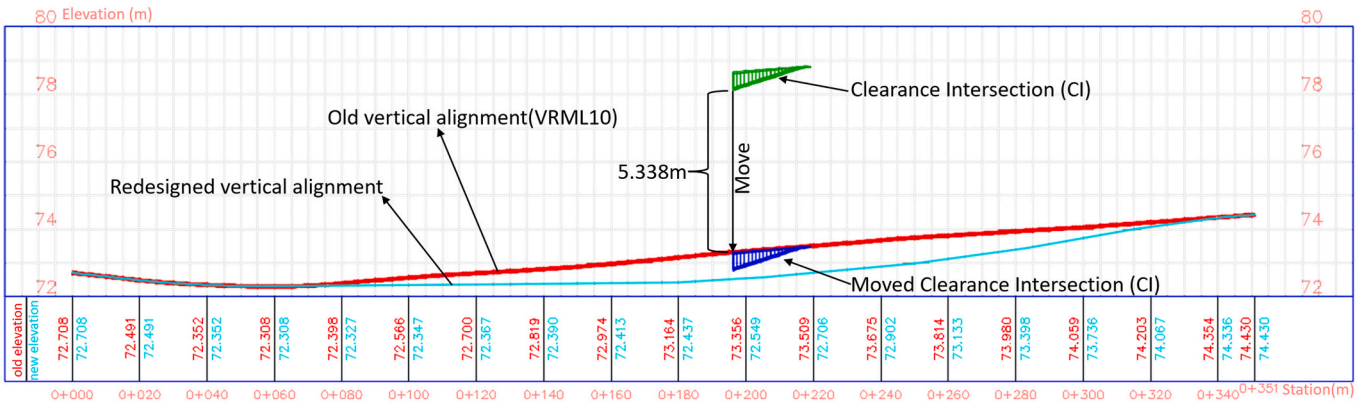

Fig. 26. Redesign of the underpass road.

effective clearance check and redesign methods for the existing low-level underpass road in the main road widening project using online map data without a field survey.

However, from the evaluation perspective, a field survey should be conducted in future research to evaluate the proposed method. In addition to quantitative evaluation, qualitative comparisons between

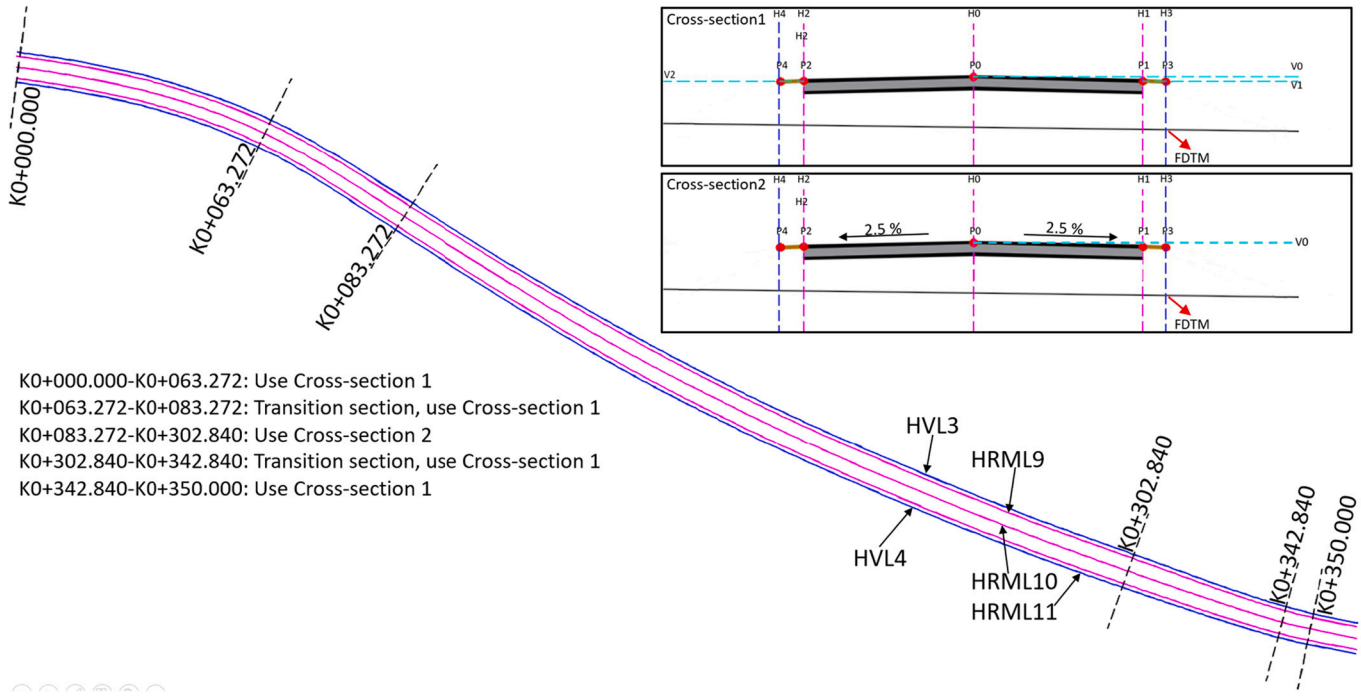

Fig. 27. BIM model of the redesigned underpass road.

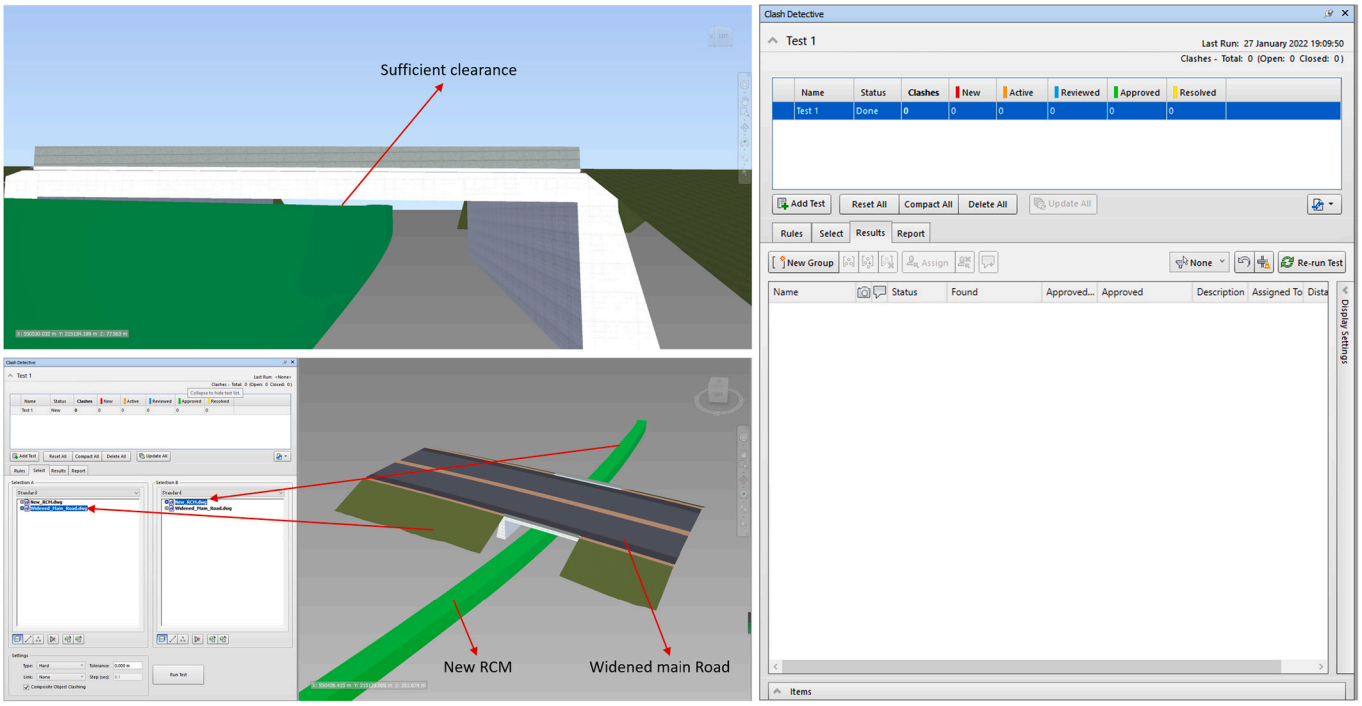

Fig. 28. Clearance check after the redesign of the underpass road.

the proposed method and other similar semi-automatic methods leveraging commercial software should be performed in future research. Several focus groups and interviews can be held with some experts to evaluate the proposed method and other existing methods. From the perspective of applications, overpass roads also should be considered in addition to underpass roads. Furthermore, the digital twin method of roads, bridges, tunnels and traffic safety facilities should be employed comprehensively to assist more road widening applications.

Declaration of Competing Interest

The authors declare that they have no known competing financial interests or personal relationships that could have appeared to influence the work reported in this paper.

Acknowledgement

This study is supported by the Major Science &Technology Project of

Hubei (Grant No. 2020ACA006).

References

[1] G.A. Adeyemi, O.G. Gbolahan, M. Markus, S.O. Edeki, Geospatial analysis of building demolition during road expansion project in Ado-Odo OTA settings, Int. J. Civil Eng. Technol. 9 (12) (2018) 303–314. https://iaeme.com/Home/article_id/IJCIET_09_12_034.

[2] L. Barazzetti, M. Previtali, M. Scaioni, Roads detection and parametrization in integrated BIM-GIS using LiDAR, Infrastructures 5 (7) (2020), https://doi.org/10.3390/infrastructures5070055.

[3] Z.P. Bažant, Q. Yu, G.H. Li, Excessive long-time deflections of prestressed box girders. I: Record-span Bridge in Palau and other paradigms, J. Struct. Eng. (United States) 138 (6) (2012) 676–686, https://doi.org/10.1061/(ASCE)ST.1943-541X.0000487.

[4] A. Best, Keeping hoofs off hoods, Planning 83 (3) (2017) 12–18. https://www.proquest.com/docview/1876055382?accountid=14511.

[5] S.L. Birge, Highway dimensions from Photolog, Photogramm. Eng. Remote. Sens. 51 (10) (1985) 1609–1614. https://www.asprs.org/wp-content/uploads/pers/1985journal/oct/1985_oct_1609-1614.pdf.

[6] A. Broekman, P.J. Gräbe, W.J.V. Steyn, Real-time traffic quantization using a mini edge artificial intelligence platform, Transp. Eng. Aust. 4 (2021), https://doi.org/10.1016/j.treng.2021.100068.

[7] D. Cerullo, K. Sennah, H. Azimi, C. Lam, A. Fam, B. Tharmabala, Experimental study on full-scale pretensioned bridge girder damaged by vehicle impact and repaired with fiber-reinforced polymer technology, J. Compos. Constr. 17 (5) (2013) 662–672, https://doi.org/10.1061/(ASCE)CC.1943-5614.0000383.

[8] V. Charissis, J. Falah, R. Lagoo, S.F.M. Alfalah, S. Khan, S. Wang, S. Altarteer, K. B. Larbi, D. Drikakis, Employing emerging technologies to develop and evaluate in-vehicle intelligent systems for driver support: infotainment AR hud case study, Appl. Sci. (Switzerland) 11 (4) (2021) 1–28, https://doi.org/10.3390/app11041397.

[9] Z. Chen, W. Zhai, Q. Yin, Analysis of structural stresses of tracks and vehicle dynamic responses in train–track–bridge system with pier settlement, Proc. Instit. Mech. Eng. Part F: J. Rail Rapid Transit. 232 (2) (2018) 421–434, https://doi.org/10.1177/0954409716675001.

[10] A. Conine, R. Opgenorth, D. Stoutenburg, R. McGee, H.S. Colter, New day, new conflict (the challenges of water/wastewater design for a multi-billion dollar highway design-build project), in: V.F. Sever, L. Osborn (Eds.), Pipelines 2015 Conference: Recent Advances in Underground Pipeline Engineering and Construction, American Society of Civil Engineers (ASCE), 2015, pp. 498–507, https://doi.org/10.1061/9780784479360.046.

[11] C. De Santos-Berbel, M. Castro, Three-dimensional virtual highway model for sight-distance evaluation of highway underpasses, J. Surv. Eng. 144 (4) (2018), https://doi.org/10.1061/(ASCE)SU.1943-5428.0000258.

[12] F. Dembski, U. Wössner, M. Letzgus, M. Ruddat, C. Yamu, Urban digital twins for smart cities and citizens: the case study of Herrenberg, Germany, Sustainability (Switzerland) 12 (6) (2020), https://doi.org/10.3390/su12062307.

[13] Digimap, Retrieved from, https://digimap.edina.ac.uk/lidar, 2021 (Accessed date: 31 January 2022).

[14] Digimap, LiDAR Digimap Help, Retrieved from, https://digimap.edina.ac.uk/webhelp/lidar/lidardigimaphelp.htm#copyright/licence_agreement.htm, 2021 (Accessed date: 31 January 2022).

[15] Highways England, Design Manual for Roads and Bridges, CD 127 - Cross-Sections and Headrooms, Retrieved from, https://www.standardsforhighways.co.uk/prod/attachments/10442706-b592-42c8-85f8-2a0c779a8e37?inline=true, 2021.

[16] Highways England, Design Manual for Roads and Bridges, CD 358 - Waterproofing and Surfacing of Concrete Bridge Decks, Retrieved from, https://www.standardsforhighways.co.uk/prod/attachments/d618f15c-5fd3-4802-a986-aaa0581c98fa?inline=true, 2022.

[17] R.J. Fowler, J.J. Little, Automatic extraction of irregular network digital terrain models, in: Proceedings of the Annual Conference on Computer Graphics and Interactive Techniques (SIGGRAPH '79), 6th 13 (2), 1979, pp. 199–207, https://doi.org/10.1145/965103.807444.

[18] S.A. Gargoum, L. Karsten, K. El-Basyouny, J.C. Koch, Automated assessment of vertical clearance on highways scanned using mobile LiDAR technology, Autom. Constr. 95 (2018) 260–274, https://doi.org/10.1016/j.autcon.2018.08.015.

[19] G. Gräfe, High precision kinematic surveying with laser scanners, J. Appl. Geod. 1 (4) (2007) 185–199, https://doi.org/10.1515/jag.2007.021.

[20] D.J. Graham, S. Glaister, Road traffic demand elasticity estimates: a review, Transp. Rev. 24 (3) (2004) 261–274, https://doi.org/10.1080/0144164032000101193.

[21] M. Grieves, J. Vickers, Digital twin: Mitigating unpredictable, undesirable emergent behavior in complex systems, in: Transdisciplinary Perspectives on Complex Systems: New Findings and Approaches, Springer International Publishing, 2016, pp. 85–113. ISBN 9783319387567; ISBN 9783319387543.

[22] B.L. Halliday, Ngauranga gorge road overpass, Wellington, transactions of the institution of professional engineers New Zealand, Civil Eng. Sect. 12 (2) (1985) 79–86. https://search.informit.org/doi/10.3316/informit.465316486654915.

[23] M.C. Hite, R. DesRoches, R.T. Leon, Full-scale tests of bridge steel pedestals, J. Bridg. Eng. 13 (5) (2008) 483–491, https://doi.org/10.1061/(ASCE)1084-0702(2008)13:5(483).

[24] T. Horberry, M. Halliday, A.G. Gale, Bridge strike reduction: Optimising the design of markings, Accid. Anal. Prev. 34 (5) (2002) 581–588, https://doi.org/10.1016/S0001-4575(01)00055-0.

[25] M. Intignano, S.A. Biancardo, C. Oreto, N. Viscione, R. Veropalumbo, F. Russo, G. Ausiello, G. Dell'acqua, A scan-to-bim methodology applied to stone pavements in archaeological sites, Heritage 4 (4) (2021) 3032–3049, https://doi.org/10.3390/heritage4040169.

[26] J.C. Jeon, H.H. Lee, Development of displacement estimation method of girder bridges using measured strain signal induced by vehicular loads, Eng. Struct. 186 (2019) 203–215, https://doi.org/10.1016/j.engstruct.2019.01.107.

[27] F. Jiang, L. Ma, T. Broyd, K. Chen, Digital twin and its implementations in the civil engineering sector, Autom. Constr. 130 (2021), https://doi.org/10.1016/j.autcon.2021.103838.

[28] F. Jiang, L. Ma, T. Broyd, W. Chen, H. Luo, Building digital twins of existing highways using map data based on engineering expertise, Autom. Constr. 134 (2022), https://doi.org/10.1016/j.autcon.2021.104081.

[29] F. Jiang, L. Ma, T. Broyd, W. Chen, H. Luo, Digital twin enabled sustainable urban road planning, Sustain. Cities Soc. 78 (2022), https://doi.org/10.1016/j.scs.2021.103645.

[30] M. Jilun, C. Chuang, X. Shengxie, Evaluation on risk for ship collision with archbridge and crash capability of anti-collision, Open Civil Eng. J. 8 (1) (2015) 351–359, https://doi.org/10.2174/1874149501408010351.

[31] A. Justo, M. Soilán, A. Sánchez-Rodríguez, B. Riveiro, Scan-to-BIM for the infrastructure domain: generation of IFC-complaint models of road infrastructure assets and semantics using 3D point cloud data, Autom. Constr. 127 (2021), https://doi.org/10.1016/j.autcon.2021.103703.

[32] S. Kaewunruen, J. Sresakoolchai, W. Ma, O. Phil-Ebosie, Digital twin aided vulnerability assessment and risk-based maintenance planning of bridge infrastructures exposed to extreme conditions, Sustainability (Switzerland) 13 (4) (2021) 1–19, https://doi.org/10.3390/su13042051.

[33] W. Kramer, W. Martin, H. Viljoen, Demolition of Old Oak Bridge B4113: condition of a 54-year old prestressed concrete bridge, in: M.G. Alexander, H. Beushausen, P. Moyo, F. Dehn (Eds.), 5th International Conference on Concrete Repair, Rehabilitation and Retrofitting, ICCRRR Vol. 199, EDP Sciences, 2018, p. 2018, https://doi.org/10.1051/matecconf/201819906002.

[34] S.S. Lee, K.T. Kim, W.A. Tanoli, J.W. Seo, Flexible 3D model partitioning system for nD-based BIM implementation of alignment-based civil infrastructure, J. Manag. Eng. 36 (1) (2020), https://doi.org/10.1061/(ASCE)ME.1943-5479.0000725.

[35] Q. Liu, T. Wang, R.R. Souleyrette, A 3D evaluation method for rail–highway hump crossings, Comp. Aided Civil Infrastruct. Eng. 32 (2) (2017) 124–137, https://doi.org/10.1111/mice.12244.

[36] T. Machl, A. Donaubauer, T.H. Kolbe, Planning agricultural core road networks based on a digital twin of the cultivated landscape, J. Digital Landscape Architect. 2019 (4) (2019) 316–327, https://doi.org/10.14627/537663034.

[37] MathWorks, Smoothing Splines, Retrieved from, https://www.mathworks.com/help/curvefit/smoothing-splines.html, 2021 (Accessed date: 31 January 2022).

[38] S. Meža, A. Mauko Pranjić, R. Vezočnik, I. Osmokrović, S. Lenart, Digital twins and road construction using secondary raw materials, J. Adv. Transp. 2021 (2021), https://doi.org/10.1155/2021/8833058.

[39] C. Oreto, S.A. Biancardo, R. Veropalumbo, N. Viscione, F. Russo, F. Abbondati, G. Dell'acqua, BIM-LCA integration framework for sustainable road pavement maintenance practices, Int. J. Transp. Develop. Integrat. 6 (1) (2022) 1–11, https://doi.org/10.2495/TDI-V6-N1-1-11.

[40] R. Osegueda, A. Garcia-Diaz, S. Ashur, O. Melchor, S.H. Chang, C. Carrasco, A. Kuyumcu, GIS-based network routing procedures for overweight and oversized vehicles, J. Transp. Eng. 125 (4) (1999) 324–331, https://doi.org/10.1061/(ASCE)0733-947X(1999)125:4(324).

[41] A.I. Ozdagli, F. Moreu, D. Xu, T. Wang, Experimental analysis on effectiveness of crash beams for impact attenuation of overheight vehicle collisions on railroad bridges, J. Bridg. Eng. 25 (1) (2020), https://doi.org/10.1061/(ASCE)BE.1943-5592.0001503.

[42] A. Polus, M.A. Pollatschek, Criteria for widening of two-lane rural highways, Transp. Policy 11 (4) (2004) 379–385, https://doi.org/10.1016/j.tranpol.2004.06.001.

[43] B. Shan, L. Wang, X. Huo, W. Yuan, Z. Xue, A bridge deflection monitoring system based on CCD, Adv. Mater. Sci. Eng. 2016 (2016), https://doi.org/10.1155/2016/4857373. Article ID 4857373, 11 pages.

[44] H. Sharma, S. Hurlebaus, P. Gardoni, Development of a bridge bumper to protect bridge girders from overheight vehicle impacts, Comp. Aided Civil Infrastruct. Eng. 23 (6) (2008) 415–426, https://doi.org/10.1111/j.1467-8667.2008.00548.x.

[45] W.J.V.D.M. Steyn, A. Broekman, Development of a digital twin of a local road network: a case study, J. Test. Eval. 51 (1) (2021), https://doi.org/10.1520/JTE202100.43.

[46] K. Taniguchi, S. Kubota, Y. Yasumuro, Quantitative visualization of physical barriers for vulnerable pedestrians based on photogrammetry, Constr. Innov. (2022), https://doi.org/10.1108/CI-04-2021-0087.

[47] V. Tihanyi, A. Rövid, V. Remeli, Z. Vincze, M. Csonthó, Z. Pethő, M. Szalai, B. Varga, A. Khalil, Z. Szalay, Towards cooperative perception services for its: digital twin in the automotive edge cloud, Energies 14 (18) (2021), https://doi.org/10.3390/en14185930.

[48] D. Turner, R.D. Coombe, Sub-standard grade-separation, Traffic Eng. Control 27 (3) (1986) 108–114. https://trid.trb.org/view/229011.

[49] Uttlesford District Council, Statement of Common Ground on Surface Access Matters Between Stansted Airport Limited, Highways England and Essex County Council, Retrieved from, http://www.hwa.uk.com/site/wp-content/uploads/2020/10/20201207-StanstedTransportSoCG-v2-final-Appendicies.pdf, 2021 (Accessed date: 31 January 2022).

[50] D. Vines-Cavanaugh, R. Birken, M. Wang, In field application of rapid roadway inspection system using vehicle-mounted multi-modal sensing, in: F.K. Chang

(Ed.), 9th International Workshop on Structural Health Monitoring: A Roadmap to Intelligent Structures, IWSHM 2013 Vol. 1, DEStech Publications, 2013, pp. 611–619, in: https://www.dpi-proceedings.com/index.php/shm2013/article/view/22841.
[51] S.H. Wang, C.H. Tu, J.C. Juang, Automatic traffic modelling for creating digital twins to facilitate autonomous vehicle development, Connect. Sci. (2021), https://doi.org/10.1080/09540091.2021.1997914.
[52] C. Watson, S.E. Chen, H. Bian, E. Hauser, Three-dimensional terrestrial LIDAR for operational bridge clearance measurements, J. Perform. Constr. Facil. 26 (6) (2012) 803–811, https://doi.org/10.1061/(ASCE)CF.1943-5509.0000277.
[53] Y.U.V. Wikipedia, Retrieved from, https://en.wikipedia.org/wiki/YUV, 2022.
[54] N. Yazdani, M.A.D.L.F. Montero, Structural performance of impact damaged and repaired concrete bridge girder using GFRP rebars, Innovat. Infrastruct. Solutions 1 (1) (2016), https://doi.org/10.1007/s41062-016-0034-7.
[55] S. Ye, X. Lai, I. Bartoli, A.E. Aktan, Technology for condition and performance evaluation of highway bridges, J. Civ. Struct. Heal. Monit. 10 (4) (2020) 573–594, https://doi.org/10.1007/s13349-020-00403-6.
[56] W.P. Yen, G. Chen, I. Buckle, T. Allen, D. Alzamora, J. Ger, J.G. Arias, Postearthquake reconnaissance report on transportation infrastructure impact of the February 27, in: Offshore Maule Earthquake in Chile, 2011, Federal Highway Administration, 2010. Retrieved from, https://www.fhwa.dot.gov/publications/research/infrastructure/structures/11030/11030.pdf (Accessed date: 29 April 2022).
[57] G. Yu, S. Zhang, M. Hu, Y. Ken Wang, Prediction of highway tunnel pavement performance based on digital twin and multiple time series stacking, Adv. Civil Eng. 2020 (2020), https://doi.org/10.1155/2020/8824135.